nature nanotechnology

Article

https://doi.org/10.1038/s41565-025-01958-5

Tailoring the adjuvanticity of lipid nanoparticles by PEG lipid ratio and phospholipid modifications

Received: 27 April 2024

Accepted: 9 May 2025

Published online: 23 June 2025

Check for updates

Máté Vadovics[1,11], Wenchen Zhao[2,11], Emily F. Daley[1,11], Kieu Lam[2], Owen Daly[2], Khalid Rashid[3], Hailey R. Lee[3], Petra Schreiner[2], Kendall A. Lundgreen[1], Brian T. Gaudette[4], Vladimir V. Shuvaev[5], Evguenia Arguiri[5], Hiromi Muramatsu[1], András Sárközy[1], Thandiswa Mdluli[1], Junchao Xu[6], Xuexiang Han[6,10], Nina De Luna[1,7], Diana Castaño[1,7], Emily Bettini[1,7], Edit Ábrahám[8,9], Zoltan Lipinszki[8,9], Giuseppe Carlucci[3], Avinash Haridas Bansode[3], Katelyn Nguyen[3], Thuc M. Le[3], Tony Luu[3], Vladimir R. Muzykantov[5], Paul Bates[1], David Allman[4], Michael J. Mitchell[6], Michela Locci[1,7], Caius G. Radu[3], James Heyes[2] & Norbert Pardi[1]

Lipid nanoparticles (LNPs) represent the leading delivery platform for mRNA vaccines with advantageous biocompatibility, scalability, adjuvant activity and often an acceptable safety profile. Here we investigate the physicochemical characteristics and adjuvanticity of four-component LNPs. Previous vaccine studies have demonstrated that altering the ionizable lipid influences the adjuvanticity of an LNP; however, the impact of the polyethylene glycol lipid and phospholipid has received less attention. Our mRNA–LNP vaccine formulations utilized different phospholipids and varying ratios of polyethylene glycol lipid, whereas the ionizable lipid and cholesterol remained approximately constant. We demonstrate that such modifications impact the magnitude and quality of the vaccine-elicited immune responses. We also dissect the underlying mechanisms and show that the biodistribution and cellular uptake of LNPs correlate with the magnitude and quality of the immune responses. These findings support the rational design of novel LNPs to tailor immune responses (cellular or humoral focused) based on the vaccine application.

The nucleoside-modified mRNA–lipid nanoparticle (mRNA–LNP) technology is in the spotlight of vaccine development due to its success in the fight against the coronavirus disease 2019 (COVID-19)[1]. Pfizer/BioNTech's BNT162b2 and Moderna's mRNA-1273 are highly effective in preventing COVID-19-associated hospital admissions and deaths by eliciting potent antigen-specific neutralizing antibody and T cell responses[1–4]. Both vaccines utilize LNP-encapsulated N1-methylpseudouridine-containing mRNA encoding the prefusion-stabilized spike glycoprotein of SARS-CoV-2 (refs. 5,6). The use of modified nucleosides facilitates decreased innate immune sensing of the mRNA and a high level of antigen production[7,8]. The ionizable lipid-containing LNPs function as a safe and efficient delivery modality[9] and also serve as potent adjuvants[10,11]. LNPs typically have four components: ionizable lipid, cholesterol, phospholipid and PEGylated lipid incorporating polyethylene glycol (PEG). The ionizable lipid serves to encapsulate nucleic acids within the LNPs and facilitates endosomal escape of the mRNA after cellular uptake[12]. Furthermore, it promotes robust IL-6 production, and the elicitation of neutralizing

A full list of affiliations appears at the end of the paper. e-mail: pnorbert@pennmedicine.upenn.edu

https://doi.org/10.1038/s41565-025-01958-5

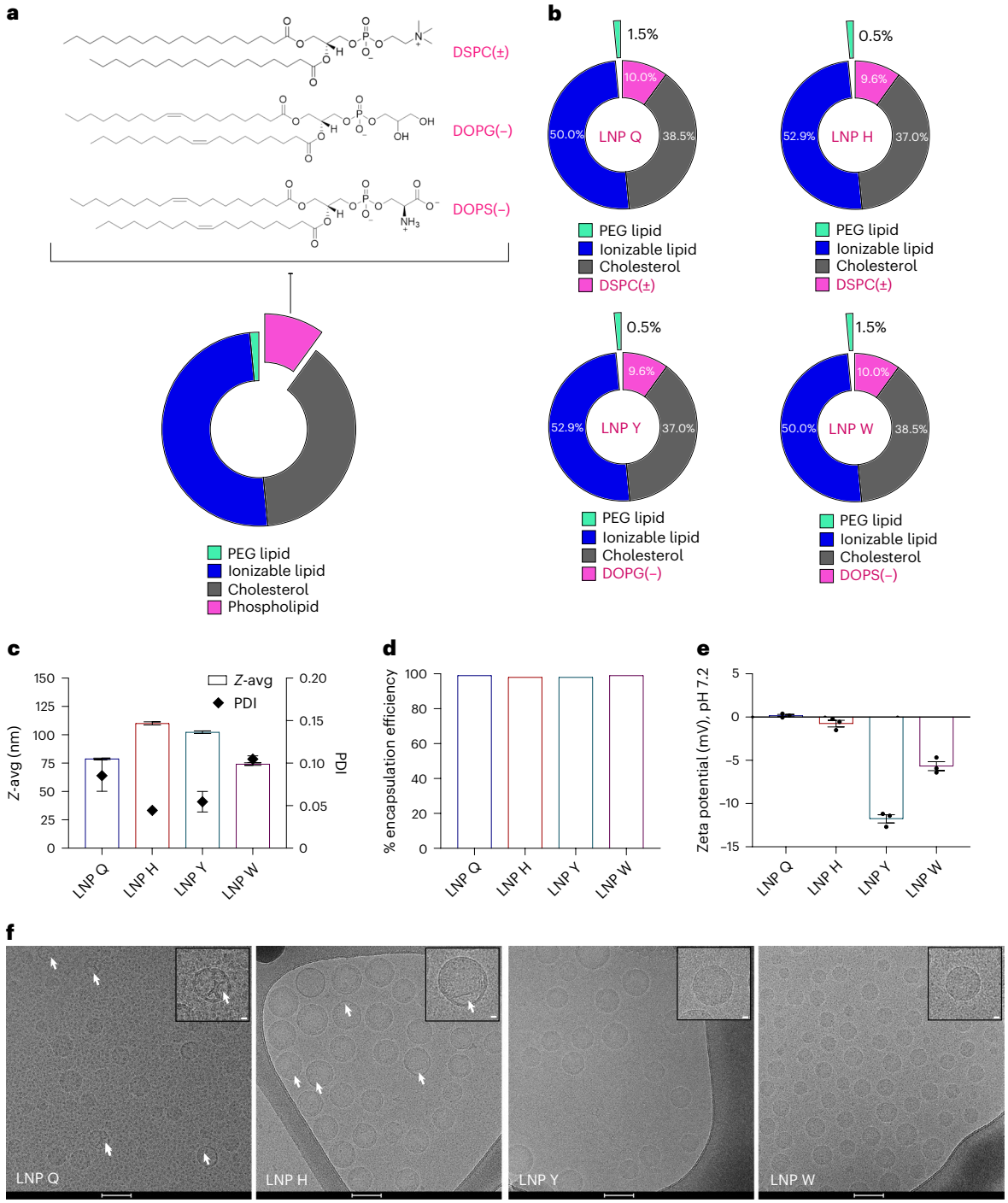

Fig. 1 | Design and characterization of S-2P mRNA–LNP variants. **a**, Representative LNP composed of a PEG-conjugated lipid, ionizable lipid, cholesterol and phospholipid, where the phospholipid is either DSPC (zwitterionic), DOPG (negatively charged) or DOPS (negatively charged). **b**, Lipid composition of each S-2P mRNA–LNP variant (LNP Q, H, Y and W). **c**, Particle size (*Z*-avg) and polydispersity index (PDI) measured by dynamic light scattering. **d**, S-2P mRNA encapsulation efficiency determined by RiboGreen. **e**, Surface charge of S-2P mRNA–LNP measured by Zetasizer. **f**, Representative cryo-transmission electron microscopy images of S-2P mRNA–LNP. Scale bar, 100 nm (main image); 10 nm (inset). The white arrows show the bleb structures. The cryo-transmission electron microscopy analysis was performed twice using either Luc or S-2P mRNA, with 15 images captured in each experiment. All data are presented as mean ± s.e.m. The bar diagrams (**c**–**e**) represent three technical replicates of the same sample.

antibodies as a response to vaccination with mRNA–LNPs[10]. Cholesterol provides rigidity and stabilizes the LNPs[13]. Phospholipids contribute to a longer circulation time, influence overall stability in solution[13] and can be optimized for better tissue-specific targeting of LNPs[14–16]. PEG lipids can impact size and polydispersity, particle stability, nucleic acid encapsulation efficiency, circulation half-life, in vivo distribution and transfection efficiency[13].

By refining the LNP formulation, it may be possible to influence not only the magnitude but also the quality of mRNA–LNP vaccine-elicited immune responses. In previous work, we showed that the ionizable lipid component of LNPs is important for its adjuvant effect[10]. Ionizable lipid optimizations can improve the safety and immunogenicity profile of mRNA–LNP vaccines[17]. In a more recent study, an adjuvant lipidoid was developed that enhances the adjuvanticity of mRNA–LNP

vaccines[18]. Other recent publications have reported how the phospholipid and PEG lipid modifications influence the physicochemical properties and biodistribution of LNPs[16,19–24]. However, the impact of phospholipid and PEG lipid on the adjuvanticity of LNPs has not been thoroughly investigated.

Here we studied four LNPs with different phospholipids and varying amounts of PEG lipids to determine how these variations affect the adjuvant activity of the LNP in the context of vaccination. We generated mRNA vaccines by formulating viral antigen-encoding nucleoside-modified mRNA into the four different LNPs, determined physicochemical properties of the mRNA–LNPs and evaluated vaccine-induced immune responses in mice. We demonstrated that the type of phospholipids and ratios of PEG lipids influence the adjuvant properties of LNPs and affect not only the magnitude but also the quality of the induced immune responses. More specifically, we show examples of how novel LNPs can be designed to preferentially elicit potent antibody responses or $CD8^+$ T cell responses for mRNA vaccines targeting infectious diseases or cancer. We then provide mechanistic data suggesting that adjuvanticity is probably driven by the biodistribution of mRNA vaccines, LNP-driven efficiency of mRNA uptake and endosomal release, and the inflammatory properties of mRNA–LNPs. This study shows that the optimization of LNPs can enhance mRNA vaccine efficacy and tailor the adjuvanticity for infectious diseases and potentially for cancer therapy.

LNP design and characterization

All LNPs examined in this study are composed of an ionizable lipid[25], cholesterol, a PEG lipid and a phospholipid, where the phospholipid is either distearoyl-*sn*-glycero-3-phosphocholine (DSPC), 1,2-dioleoyl-*sn*-glycero-3-phosphoglycerol (DOPG) or 1,2-dioctadecenoyl-*sn*-glycero-3-phosphoserine (DOPS). In contrast to the FDA-approved COVID-19 mRNA vaccines that contain DSPC, a zwitterionic phospholipid with saturated tails, both DOPG and DOPS are anionic phospholipids with oleyl chains containing a *cis* double bond (Fig. 1a).

LNP Q, our benchmark composition, has demonstrated a safe and highly immunogenic profile in a Phase 2 COVID-19 mRNA vaccine trial[26]. Setting this as the base composition (ionizable lipid, cholesterol, DSPC and PEG at a molar ratio of 50:38.5:10:1.5, respectively), we generated and characterized a panel of LNPs (F-T) by titrating PEG lipid and keeping the amount of ionizable lipid, cholesterol and DSPC nearly constant (Supplementary Table 1). Using influenza virus hemagglutinin (HA)-encoding nucleoside-modified mRNA, we found that LNPs containing lower PEG concentrations elicited stronger antigen-specific antibody responses (Supplementary Fig. 1 and Supplementary Table 2). On the basis of these results, we selected LNP H, which uses a PEG lipid ratio of 0.5%. We next sought to explore the influence of phospholipid charge on these formulations. Previous LNP delivery studies have demonstrated that when administered intravenously, negatively charged LNPs traffic primarily to the spleen[15,16]. We hypothesized that delivery to a secondary lymphoid organ would be advantageous for vaccine applications; therefore, we selected two commonly used negatively charged phospholipids, namely, DOPG and DOPS[16]. In addition, our studies used intramuscular (i.m.) administration, which can alter LNP trafficking compared with intravenous delivery[9]. After the formulation of LNPs (V-Z) using these negatively charged phospholipids and varying the PEG ratios (Supplementary Table 1), we selected LNPs for further study based on lower PEG ratios and acceptable size profiles. When formulating DOPS with 0.5% PEG (LNP V), the *Z*-average was 146 nm—much higher than the previously reported optimal sizing of LNPs for robust adjuvanticity in mice, which is around 100 nm (ref. 27). Larger-sized LNP formulations (>120 nm) may present additional chemistry, manufacturing and control challenges for any potential clinical product due to difficulties in filtration and the potential for further particle size growth on longer-term storage or freeze–thaw. Therefore, we returned to the PEG ratio of 1.5% for this phospholipid, which had an acceptable *Z*-average of 75 nm for LNP W (DOPS, 1.5% PEG lipid). In summary, four LNP formulations were selected for adjuvanticity and mechanistic studies. These formulations include LNP Q (1.5% PEG, DSPC) as the control and LNP H (0.5% PEG, DSPC), LNP Y (0.5% PEG, DOPG) and LNP W (1.5% PEG, DOPS).

For most subsequent studies with the selected LNPs, we used the prefusion-stabilized version of the spike glycoprotein (SARS-CoV-2 prefusion-stabilized spike (S-2P)) of the Wuhan strain of SARS-CoV-2 (ref. 28). Lipid components of the S-2P mRNA–LNPs are depicted in Fig. 1b and Supplementary Table 1. All LNPs reported a narrow size distribution and polydispersity (Fig. 1c and Supplementary Fig. 3a,b) and high encapsulation efficiency (Fig. 1d and Supplementary Fig. 3c). Despite differences in phospholipid structures, similar particle sizes were observed with LNPs made with the same lipid molar ratios. Smaller particles were obtained with 1.5% PEG (74–79 nm) compared with those with 0.5% PEG (102–110 nm; Fig. 1c, Supplementary Fig. 3a and Supplementary Table 1). All S-2P mRNA–LNPs were stable for at least 12 weeks at −80 °C (Supplementary Fig. 3d). The apparent pKa was determined to be ~6.3 for all the LNPs, driven primarily by the use of the same ionizable lipid across all the LNPs (Supplementary Fig. 3e). By design, LNPs containing anionic phospholipids (LNP Y and LNP W) exhibited a negative surface charge at pH 7.2 (Fig. 1e and Supplementary Fig. 3f). Notable differences were observed in the particle morphology of LNPs containing different phospholipids by cryo-transmission electron microscopy. DSPC-containing formulations appeared to have more 'bleb' structures, probably due to this phospholipid's saturated tails promoting cylindrical geometry and a bilayer phase in particles[29–31] (Fig. 1f and Supplementary Table 3). On the other hand, DOPG and DOPS contain *cis* double bonds in their oleyl chains that promote a 'cone-shaped' geometry and the inverse hexagonal phase in particles[32].

LNP formulation impacts humoral and cellular immune responses

To investigate the impact of different types of phospholipid and the PEG lipid ratio on the adjuvant properties, mice were injected with S-2P nucleoside-modified mRNA–LNPs via i.m. administration (Fig. 2a). All formulations induced high levels of SARS-CoV-2 spike receptor-binding domain (RBD)-specific IgG that demonstrated robust neutralizing activity (Fig. 2b,c). However, at 4 weeks post-immunization, LNP H demonstrated more than a twofold increase in antibody levels and neutralizing activity compared with LNP Y and LNP W. By 16 weeks post-immunization, LNP H induced more than threefold higher levels of antigen-specific IgG compared with LNP Q, LNP Y and LNP W, and fourfold higher neutralization compared with LNP W.

Because our LNP formulations elicited varied antibody responses, we examined not only the magnitude but also the quality of the humoral immune response by assessing the levels of IgA and various IgG subtypes (Supplementary Fig. 4a). Our analysis revealed that diverse LNP compositions can impact IgG1/IgG2a ratios (Supplementary Fig. 4b).

Most successful vaccine approaches rely on the generation of memory B cells (MBCs) and long-lived plasma cells (LLPCs)[33]. Although MBCs can mount rapid recall responses on secondary exposure, LLPCs residing in the bone marrow contribute to protection from infection by a persistent production of antigen-specific antibodies. To examine the magnitude and quality of antigen-specific LLPC and MBC responses, at 16 weeks post-vaccination, the RBD-specific splenic MBCs and bone marrow LLPCs were identified by flow cytometry. Similar to the humoral immune responses, LNP H induced the largest amount of antigen-specific MBCs and LLPCs out of the four LNPs (Fig. 2d,e and Supplementary Fig. 5), as well as the highest number of IgG1-, IgG2a- and IgG2b-producing RBD-specific antibody-secreting cells quantified by ELISpot (Fig. 2f).

We previously demonstrated that nucleoside-modified mRNA–LNP vaccines induce robust antigen-specific $CD4^+$ and $CD8^+$ T cell responses in mice[34]. To gain further insights into the cellular immune

https://doi.org/10.1038/s41565-025-01958-5

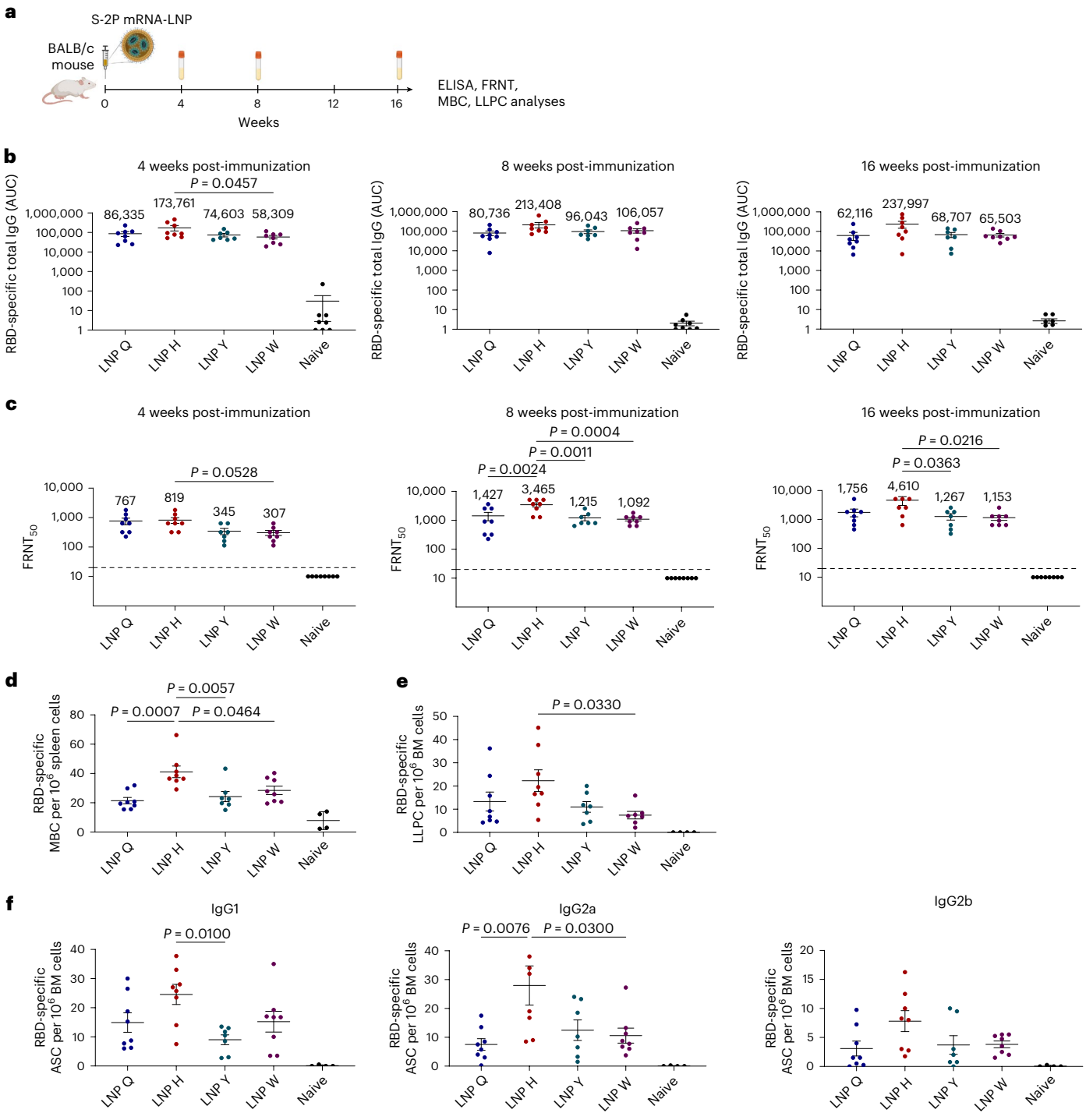

Fig. 2 | LNP formulations with different phospholipids and PEG lipid ratios induce distinct humoral, LLPC and MBC immune responses. a, Schematic of the experiments evaluating the humoral, LLPC and MBC immune responses. BALB/c mice received a single i.m. immunization with 5 μg of S-2P mRNA encapsulated in different LNP formulations. Serum samples were collected for ELISA and FRNT assays at 4 weeks, 8 weeks and 16 weeks post-injection. At 16 weeks post-injection, LLPCs and MBCs were analysed from the bone marrow and spleen, respectively. **b**, RBD-specific total IgG levels were determined by ELISA using mouse serum. AUC with a cut-off value of the average background plus three standard deviations are shown. **c**, Neutralizing antibody levels were measured by a VSV-based pseudovirus neutralization assay. $n = 8$ mice per group in a single experiment. For the ELISA and FRNT assays, samples from a single timepoint were analysed in one experiment with two technical replicates. The dashed line represents the lower limit of detection. **d**,**e**, MBCs (**d**) and LLPCs (**e**) in the spleen and bone marrow respectively, were analysed 16 weeks post-immunization by flow cytometry. RBD-specific MBCs (IgD^-Dump[CD4, CD8a, Ter-119, F4/80]$^-CD19^+B220^+CD38^+GL7^-$RBD-AF647$^+$/RBD-PE$^+$) and antigen-specific LLPCs (IgD^-Dump[CD4, CD8a, Ter-119, F4/80]$^-B220^-CD138^+$RBD-AF647$^+$/RBD-PE$^+$) are shown. In the LNP W group, one animal displayed an extremely low event count, and that particular animal was excluded from the LLPC analysis. **f**, Quantification of bone marrow (BM) RBD-specific IgG1, IgG2a and IgG2b antibody-secreting cells (ASCs) by ELISpot Assay at 16 weeks post-immunization. For **d**–**f**, $n = 8$ mice per group and $n = 4$ per naive group combined from two independent experiments. For **b**–**f**, each symbol represents one animal, and the data represent mean ± s.e.m. One-way analysis of variance (ANOVA) with Tukey's multiple comparisons test was performed. One animal in the LNP Y group died during the experiments. Panel **a** created with BioRender.com.

https://doi.org/10.1038/s41565-025-01958-5

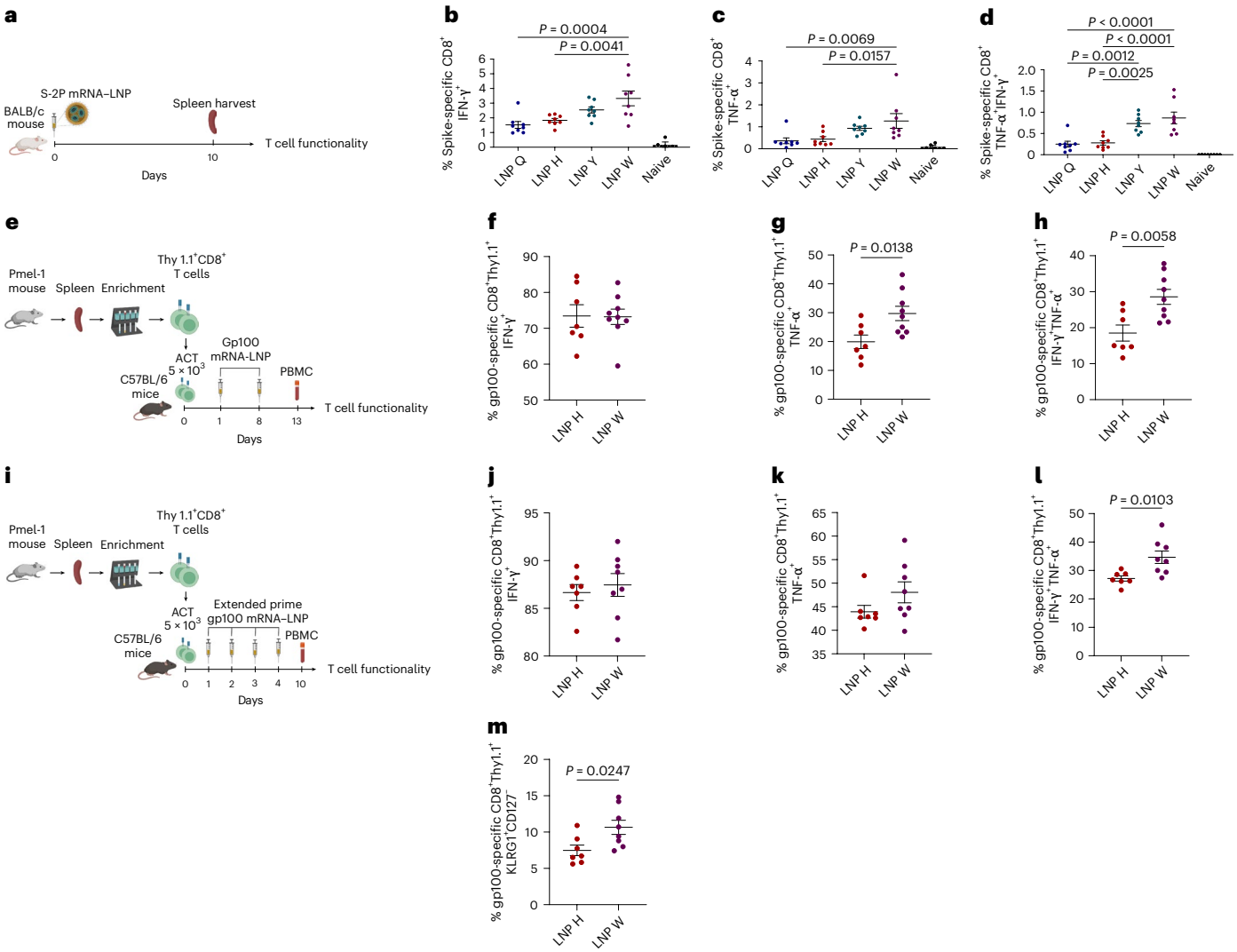

Fig. 3 | Phospholipids and PEG lipids have an impact on antigen-specific CD8⁺ T cell responses. a, Schematic of the experiment on spike-specific CD8⁺ T cell responses. BALB/c mice received a single i.m. immunization with 5 μg of S-2P mRNA encapsulated in different LNP formulations. **b**–**d**, Splenocytes collected from animals 10 days after injection were stimulated with SARS-CoV-2 spike protein peptide pool and cytokine production by CD8⁺ T cells was assessed by flow cytometry. $n = 8$ mice per group combined from two independent experiments. Each symbol represents one animal, and the data represent mean ± s.e.m. One-way ANOVA with Tukey's multiple comparisons test was performed. **e**, Schematic of the experiment investigating gp100-specific CD8⁺ T cell responses following a prime–boost injection. CD8⁺ T cells were purified from the spleens of Pmel-1 TCR/Thy1.1 transgenic mice and transferred via a tail-vein injection into naive, lymphoreplete C57BL/6 recipient mice. Mice received 1-μg prime one day later (day 1) and 1-μg boost (on day 8) of mRNA–LNP encoding full-length murine gp100 via i.m. administration. **f**–**h**, PBMCs collected 5 days post-boost were stimulated with the $gp100_{25–33}$ peptide, and cytokine-producing antigen-specific CD8⁺ Thy1.1⁺ T cell responses were analysed by flow cytometry. $n = 8$ per LNP H group and $n = 9$ per LNP W group in a single experiment. In cases of misinjection of CD8⁺ and Thy1.1⁺ T cells, the data were excluded. **i**, Schematic of the experiment investigating gp100-specific CD8⁺ T cell responses after extended prime injection. After transferring enriched Pmel-1 CD8⁺ Thy1.1⁺ T cells into naive mice, four daily i.m. injections of 1.25 μg of gp100 mRNA–LNP were administered. **j**–**l**, PBMCs collected from animals 6 days after the last injection were stimulated with murine $gp100_{25-33}$ epitope peptide and antigen-specific CD8⁺ and Thy1.1⁺ T cell responses were evaluated by flow cytometry. $n = 7$ per LNP H group and $n = 8$ per LNP W group in a single experiment. **m**, Proportion of KLRG1⁺CD127⁻ effector T cells. $n = 7$ per LNP H group and $n = 8$ per LNP W group in a single experiment. In **f**–**h** and **j**–**m**, each symbol represents one animal, and the data represent mean ± s.e.m. An unpaired two-sided t-test was performed. Panels **a**, **e** and **i** created with BioRender.com.

responses, we investigated the T cell responses induced by different mRNA–LNPs. Mice were injected via i.m. administration and spike-specific CD4⁺ and CD8⁺ T cell responses were evaluated after 10 days using intracellular cytokine staining and flow cytometry (Fig. 3a and Supplementary Fig. 6). All mRNA–LNPs elicited antigen-specific CD8⁺ and CD4⁺ T cells expressing type 1 (Th1) immune response cytokines, including interferon (IFN)-γ and tumour necrosis factor (TNF)-α (Fig. 3b–d and Supplementary Fig. 7). There was no difference in the magnitude of antigen-specific CD4⁺ T cell responses (Supplementary Fig. 7). Interestingly, LNP W induced higher CD8⁺ T cell responses compared with the other LNP formulations (Fig. 3b–d).

Besides being important players in anti-viral responses, CD8⁺ T cells are also critical components of the adaptive immune response against cancer, playing key roles in recognizing and eliminating tumour cells[35,36]. Building on this, we evaluated T cell responses in mice following vaccination with an mRNA–LNP cancer vaccine utilizing gp100, an extensively studied melanoma-associated antigen. We selected LNP H and LNP W for comparison in these experiments, due to LNP H eliciting the highest humoral immune response, and LNP W showing superior capacity to elicit a CD8⁺ T cell response. To model T cell response at the level of endogenous precursor frequencies, we adoptively transferred a physiologically relevant number of naive gp100-specific CD8⁺ T cells

(5×10^3) from Pmel-1 mice into non-lymphodepleted mice. The following day, mice were immunized via i.m. administration with a prime and a week later with a boost bolus dose of the gp100 mRNA–LNP vaccine. We assessed the antigen-specific $CD8^+$ T cell responses 5 days after booster immunization (Fig. 3e and Supplementary Fig. 8). In line with the data obtained with the S-2P antigen, LNP W induced a significantly higher frequency of antigen-specific $CD8^+$ T cells producing TNF-α, as well as polyfunctional $CD8^+$ T cells that produced both IFN-γ and TNF-α compared with LNP H (Fig. 3f–h). In a subsequent experiment, we compared LNP W and LNP H using an extended priming immunization protocol where the total dose (5 μg) was divided into four equal daily doses (Fig. 3i). This strategy of prolonging the exposure of the immune system to antigen has been demonstrated to enhance $CD8^+$ responses[37]. LNP W elicited significantly higher polyfunctional TNF-α- and IFN-γ-producing antigen-specific $CD8^+$ T cells compared with LNP H (Fig. 3j–l), and had an increased proportion of $KLRG1^+CD127^-$ effector T cells (Fig. 3m). This confirmatory finding using a second antigen underscores the capacity of LNP W to deliver strong adjuvant activity that fosters $CD8^+$ T cell responses.

In summary, LNP H containing DSPC phospholipid and 0.5% PEG lipid ratio outperformed the other formulations in both humoral immune responses and in the number of LLPCs and MBCs, whereas LNP W containing DOPS phospholipid and 1.5% PEG lipid ratio demonstrated the most robust antigen-specific $CD8^+$ T cell responses.

Phospholipids and PEG lipid ratio influence LNP biodistribution

To understand the mechanism driving the different immune responses induced by various LNP compositions, we analysed the in vivo duration and biodistribution of protein production from different mRNA–LNPs after i.m. administration using an in vivo imaging system (IVIS). Although all LNPs produced a robust bioluminescent signal, we observed different distribution profiles (Fig. 4a and Supplementary Fig. 9). The overall bioluminescence signal measured across the full body of each mouse was over three times higher with LNP Q or LNP H containing zwitterionic phospholipids, compared with LNP Y and LNP W containing anionic phospholipids (Fig. 4b,c). However, at the injection site muscle, we could measure at least 2.5-fold higher protein production in mice injected with LNP H compared with the other three groups (Fig. 4b,c). Because IVIS does not reveal detailed organ-specific data, we evaluated the firefly luciferase (Luc) activity within various organs of mice injected via i.m. administration. The liver, spleen and draining lymph nodes (dLNs) were harvested, and Luc activity, mRNA levels and lipid content were measured from the various organs at 4 h and 3 days post-administration. After 4 h, Luc production normalized to the total protein was predominantly found in the dLNs (Fig. 4d). LNP H demonstrated twofold higher Luc expression in dLNs compared with all other formulations, but considerable amounts were also detected in the spleen and persisted at least 3 days post-injection (Fig. 4e). Meanwhile, expression in the liver was the highest with LNP Q, followed by LNP H at 4 h post-dose (Fig. 4d), whereas LNP Y and W (containing anionic phospholipids) showed low expression in the liver. To evaluate individual components of the mRNA–LNPs, we independently assessed the mRNA and ionizable lipid present in the liver and spleen following the injection of Luc mRNA–LNPs. Corroborating the Luc protein liver expression profile, mRNA and ionizable lipid levels were more than threefold higher in the liver following the administration of LNP Q and H, compared with LNP Y and W at 4 h post-injection (Fig. 4f,h). In the spleen, LNP H demonstrated at least threefold higher Luc mRNA and ionizable lipid levels compared with all other formulations at 4 h and 3 days post-injection (Fig. 4f–i).

Separately, we performed enzyme-linked immunosorbent assay (ELISA) for eGFP protein using tissue lysates. eGFP protein levels measured at 4 h and 3 days post-injections (Supplementary Fig. 10) were mostly consistent with the data obtained with Luc mRNA–LNPs (Fig. 4d,e). To further validate our LNP liver biodistribution results, we used a positron emission tomography reporter gene approach. This micropositron emission tomography/computed tomography imaging revealed significant liver uptake of LNP H and LNP Q compared with LNP Y and LNP W at 4 h post-injection (Supplementary Fig. 11), supporting our previous findings. Additionally, the positron emission tomography reporter gene approach may support future studies in quantifying LNP biodistribution not only in the liver (as shown here) but also potentially in secondary lymphoid organs in larger animal models and, eventually, in humans.

To understand the differences in liver targeting amongst our LNPs, we examined the protein corona to see if apolipoprotein E (ApoE) binding was playing a role[38–40]. Contrary to our expectations, we found that LNPs containing negatively charged phospholipids (LNP Y and LNP W) demonstrated high levels of ApoE binding (Supplementary Fig. 12), whereas LNP H exhibited the lowest ApoE binding. We also examined the presence of other HDL proteins including ApoA-1, ApoA-4 and ApoB in the protein corona. Interestingly, LNP Y and W also had higher ApoA-1 and ApoB binding, but not ApoA-4. Overall, there seem to be more HDL bound to LNP Y and W, suggesting its poor liver uptake may be mediated by other mechanisms.

LNP composition alters in vitro uptake and in vivo inflammation

To understand the mechanisms responsible for the distinct immune responses triggered by our various LNP compositions, we analysed their in vitro and in vivo cellular uptakes. The LNPs containing DSPC, LNP Q and LNP H, were taken up more readily by DC2.4 cells (Fig. 5a,b) and human-monocyte-derived dendritic cells (HuMDDCs; Fig. 5c,d), whereas the LNPs containing negatively charged phospholipids, LNP Y and LNP W, had low cellular uptake. In particular, LNP H had significantly higher uptake than all other formulations in DC2.4; in HuMDDCs, it demonstrated significantly higher uptake compared with LNP Y and LNP W. In vivo, we examined the immune cell infiltration into the dLNs and their uptake of mRNA–LNPs[41]. We evaluated different subtypes of DC, including dermal DCs, conventional type 1 and conventional type 2 DCs, as well as inflammatory monocyte and macrophage numbers.

Fig. 4 | Phospholipid and PEG lipid ratio influence the biodistribution of LNPs. **a**–**c**, In vivo imaging studies with Luc mRNA–LNPs. BALB/c mice received a single i.m. injection with 3 μg of Luc mRNA encapsulated in different LNP formulations, and bioluminescence was monitored for 11 days. **a**, Representative IVIS images taken at 4 h post-immunization with Luc mRNA–LNP. **b**,**c**, Quantification of the bioluminescent signal (**b**) and AUC (**c**) after Luc mRNA–LNP injection. $n = 5$ mice per group in a single experiment. In **b** and **c**, the left panel shows the bioluminescence signal of the whole body of the mice, whereas the right panel shows the bioluminescence signal of the injection site. **d**–**i**, Organ distribution of Luc mRNA–LNP encapsulated in different LNPs. BALB/c mice received a single i.m. injection with 5 μg of Luc mRNA encapsulated in different LNP formulations, and bioluminescence, mRNA and ionizable lipid amount were monitored in the liver, spleen and dLNs after 4 h and 3 days post-injection. **d**, Bioluminescence signal at 4 h post-injection in the liver, spleen and dLNs. **e**, Bioluminescence signal at 3 days post-injection in the liver, spleen and dLNs. In **d** and **e**, a quantitative expression as luminescence unit per mg of protein values are shown. $n = 5$–6 mice per group in a single experiment. **f**, mRNA amount at 4 h post-injection in the liver and spleen. **g**, mRNA amount at 3 days post-injection in the liver and spleen. **h**, Ionizable lipid amount at 4 h post-injection in the liver and spleen. **i**, Ionizable lipid amount at 3 days post-injection in the liver and spleen. In **f**–**i**, the quantitative amounts as pg mg^{-1} tissue values are shown. The amounts of mRNA and ionizable lipids could not be measured in the dLNs due to their limited size. $n = 5$ mice per group in a single experiment. In **c**–**i**, each symbol represents one animal; in **b**, each symbol represents a group of animals; in **b**–**i**, the data represent mean ± s.e.m. One-way ANOVA with Tukey's multiple comparisons test was performed. In **h**–**i**, the dashed line represents the lower limit of detection.

https://doi.org/10.1038/s41565-025-01958-5

At 24 h, we observed a higher absolute number of conventional type 1 DCs in the dLNs in mice injected with LNP H compared with the other LNP formulations (Supplementary Figs. 13 and 14), and at 48 h, a significant difference was observed between LNP Q and LNP Y in dermal DCs. However, when we analysed LNP uptake by these immune cells, there was no significant difference between the LNP formulations (Supplementary Figs. 14 and 15).

After LNP uptake, the mRNA must escape into the cytosol for translation into a protein[42]. In our RNA FISH experiments (Fig. 5e–h), the confocal imaging of DC2.4 cells (Fig. 5e,f) revealed that mRNA

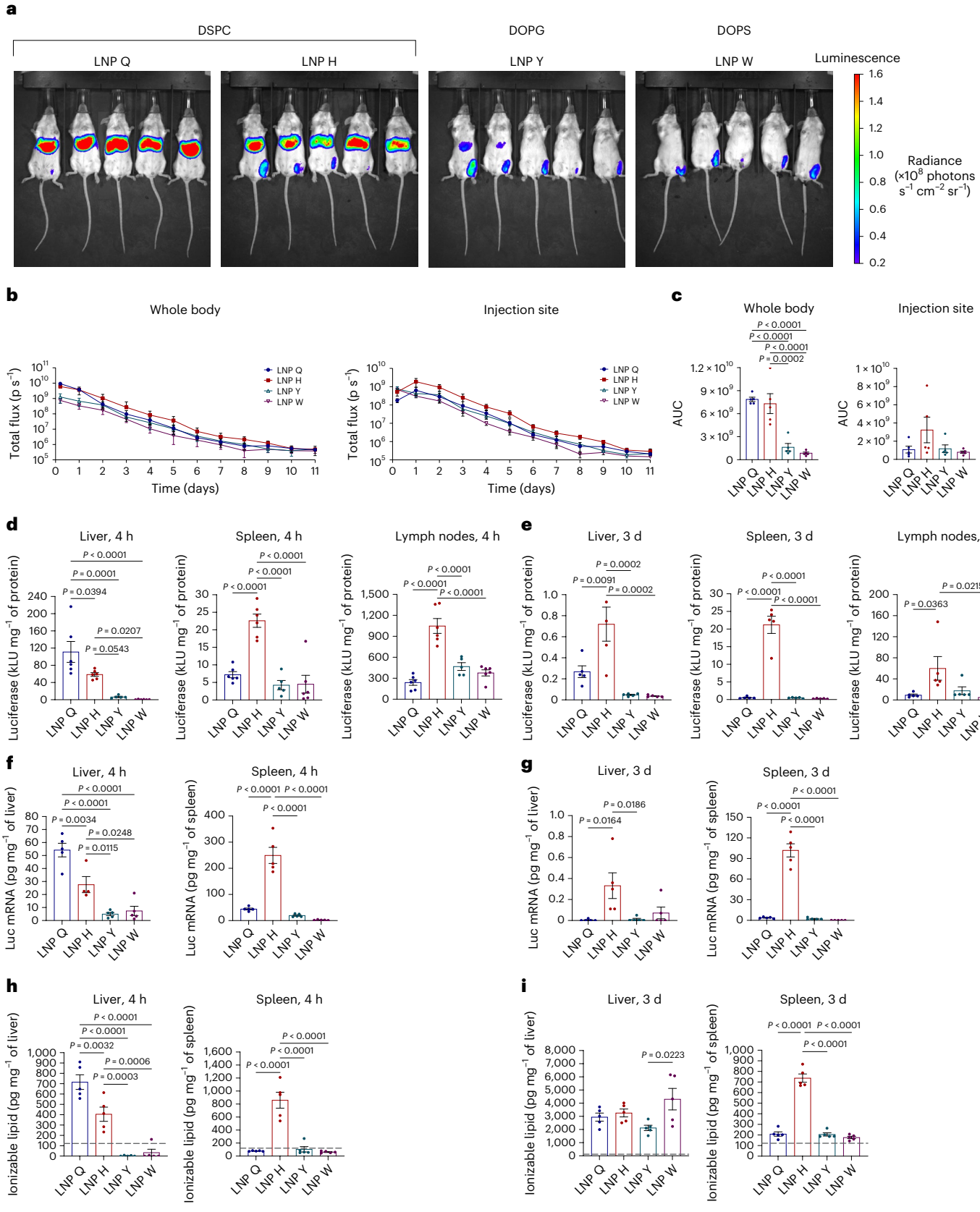

https://doi.org/10.1038/s41565-025-01958-5

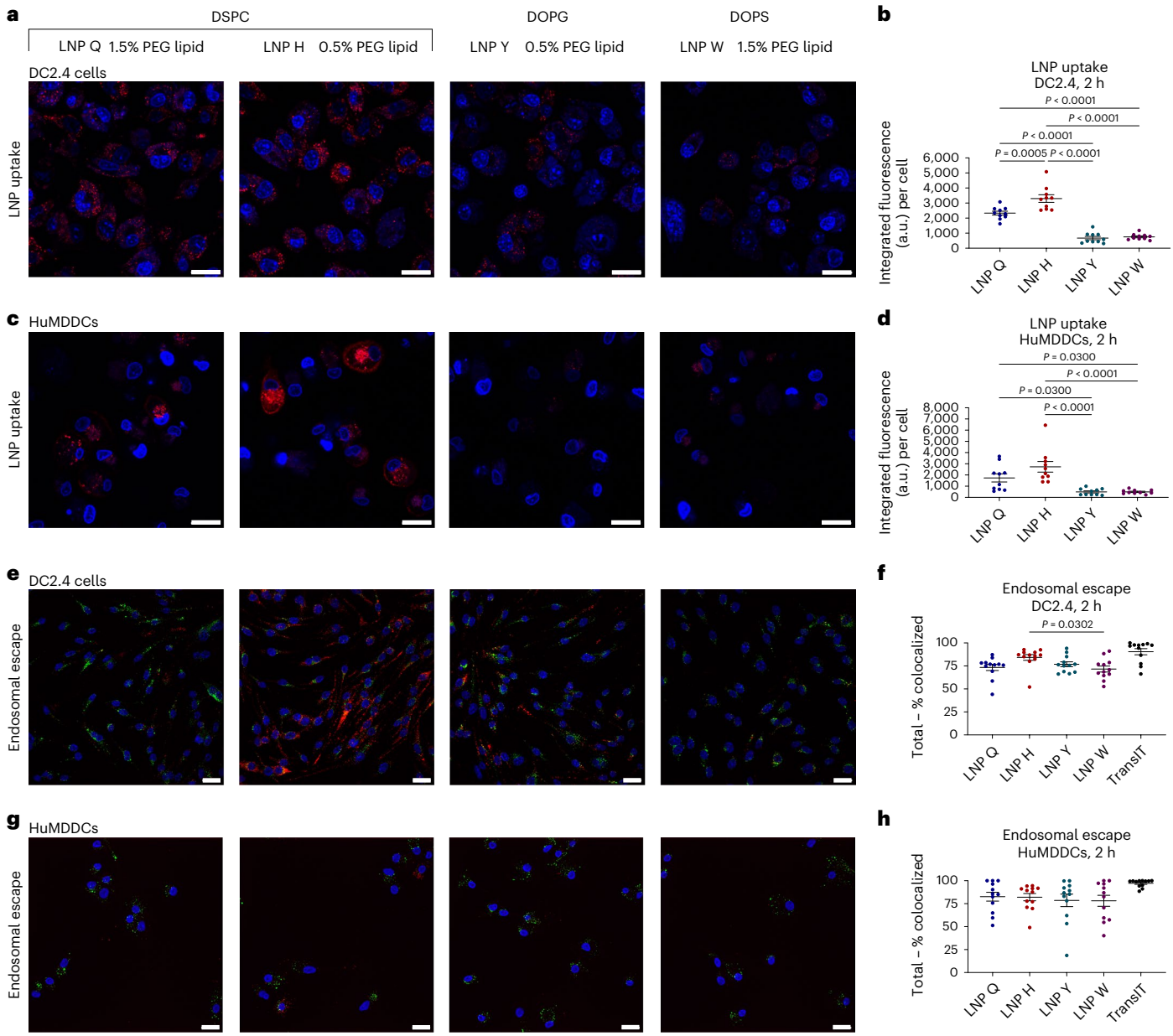

Fig. 5 | In vitro mRNA–LNP cellular uptake and mRNA endosomal escape. **a**, Representative images of LNP uptake by DC2.4 cell line. DiI-labelled LNP formulations were administered to DC2.4 cells at 500 ng ml^{-1} for 2 h. After DiI LNP exposure (red), the cells were stained with Hoescht 33342 nuclear stain (blue), washed and subsequently imaged using a laser scanning confocal microscope. **b**, LNP uptake was quantified by measuring the integrated fluorescence of DiI signal divided by the number of nuclei per image using Fiji imaging software. **c**,**d**, Representative images (**c**) and quantification (**d**) of LNP uptake by HuMDDCs. **e**,**f**, Representative images (**e**) and quantification (**f**) of mRNA colocalization with endolysosome in DC2.4 cells. Endosomal escape was evaluated by administering Luc-encoding mRNA–LNPs to DC2.4 cells for 2 h. The samples were fixed, permeabilized and stained using antibodies against EEA1 and LAMP1 (green), followed by RNA FISH probes for Luc mRNA (red). The cell nuclei were then stained with DAPI (blue). Endosomal escape values are represented by Total − %colocalized mRNA signal with the EEA1/LAMP1 signal. Colocalization is quantified by measuring the Manders colocalization coefficient after image thresholding. This was performed using Fiji. mRNA transfected with the TransIT transfection reagent is shown as a positive control. **g**,**h**, Representative images (**g**) and quantification (**h**) of of mRNA colocalization with endolysosome in HuMDDCs. Scale bar, 20 nm. The experiments were performed twice independently. Each independent study for LNP uptake included five technical replicates (individual images) per group, whereas each independent study for mRNA endosomal escape included six technical replicates (individual images) per group. For **b**, **d**, **f** and **h**, each symbol represents one image in two independent experiments. Data are represented as mean ± s.e.m. One-way ANOVA with Tukey's multiple comparisons test was performed. When the RNA signal was below the detectable threshold, endosomal escape quantification was not performed. An untransfected group was included for all the LNP uptake and endosomal escape experiments as a technical control (data not shown).

encapsulated by LNP H had a higher percentage of mRNA not colocalized with an endosomal marker, implying greater endosomal escape compared with LNP W.

In addition to cellular mechanisms that may drive adaptive immune responses to mRNA–LNP vaccines, we investigated inflammatory responses in vivo. Our previous work has shown that IL-6 induction is critical for the adjuvant activity of an LNP[10]; therefore, we evaluated the immunostimulatory cytokine profile of these four LNPs in dLNs at 4 h and 24 h post-immunization (Supplementary Fig. 16). All LNPs promoted a robust cytokine/chemokine response, and significant

differences were detected between the groups for IL-6 and IL-1β at the 4-h timepoint, as well as for IL-5 at the 24-h timepoint. At the 4-h timepoint, LNP H induced the highest IL-6 cytokine level, whereas LNP W induced the highest IL-1β level. At the site of injection, we evaluated the innate immune cell infiltration to the muscle at 1 day, 3 days and 5 days post-injection (Supplementary Figs. 17 and 18). We found that neutrophils peaked on day 1, whereas macrophages and monocytes were the highest on day 5 for all formulations. Higher levels of DCs were observed for LNP H on day 1, but there were no statistically significant differences among the groups.

Conclusions

The authorization of two nucleoside-modified mRNA–LNP-based vaccines marks an important validation of this technology in vaccine innovation[1]. Our previous research has demonstrated that LNPs are not only delivery vehicles for mRNA but also possess adjuvant activity[10] that is crucial for the induction of a strong immune response against the target antigen. However, the relationship between LNP particle composition and the quality and magnitude of the elicited immune responses remains poorly understood, primarily because most LNP research has focused on the optimization of the ionizable lipid and delivery efficiency, typically after systemic administration[15,16,21,23]. By contrast, our study addressed the impact of PEG lipid ratio and the type of phospholipid on vaccine efficacy using infectious disease and cancer models after i.m. injection.

We found that LNP H, characterized by its zwitterionic DSPC phospholipid and a lower PEG lipid ratio, induced the strongest humoral immune response, resulting in higher binding antibody production, improved virus neutralization capabilities and more robust MBC and LLPC responses. These enhancements may be attributed to increased protein synthesis measured within key immune sites such as the spleen, dLNs and the vaccination site, accompanied by heightened levels of IL-6 measured in the dLNs. The size of LNP H was the largest of our four LNPs, aligning with the findings of another work in which a correlation between the LNP particle size and the antibody response in mouse models is highlighted[27]. In vitro, we also observed more efficient uptake of LNP H by DC2.4 cells and HuMDDCs, and improved ability to release endocytosed mRNA into the cytoplasm from endosomes in DC2.4 cells. This may stem from the lower PEG lipid content[43,44] of LNP H or the presence of structural features known as blebs[30], which were measured at much higher frequencies in our LNPs containing a neutrally charged phospholipid.

On the other hand, LNP W that contained the negatively charged DOPS phospholipid led to increased frequencies of IFN-γ- and TNF-α-producing spike-specific $CD8^+$ T cells using S-2P as the model antigen. Given the critical role of $CD8^+$ T cells in the elimination of cancer cells[36,45], we investigated their response to the tumour antigen gp100 and found again that LNP W yielded the highest number of IFN-γ- and TNF-α-producing $CD8^+$ T cells. Additionally, it significantly increased the frequency of antigen-specific effector T cells characterized by the $KLRG1^+CD127^-$ T cell phenotype. Our findings agree with other work that have presented that modifying LNP formulations, such as changing phospholipids or PEG lipids, can impact the efficacy of cancer vaccines[46,47]. However, these studies focused on the optimal composition and evaluating the functional outcomes in tumour models, whereas our comparative study investigated the underlying mechanisms of how the specific composition and physicochemical properties of LNPs link to immune responses.

DOPS, a form of phosphatidylserine, facilitates the targeted delivery of LNPs to immune cells by mimicking apoptotic cell markers, thereby improving cellular uptake by antigen-presenting phagocytes[48,49]. This process may contribute to the enhanced $CD8^+$ T cell responses we observed with LNP W that contains DOPS. Moreover, the role of IL-1β in $CD8^+$ T cell induction[50–52] adds another layer to our understanding of mRNA–LNP vaccine efficacy. LNP W significantly increased the production of IL-1β in the dLNs compared with other formulations 4 h post-injection. The involvement of IL-1β, as demonstrated in ref. 11, in initiating the release of other proinflammatory cytokines further supports its critical role in mRNA–LNP vaccine immunogenicity.

Overall, this work demonstrates that modifying the phospholipid identity and the PEG lipid ratio in an LNP formulation can tune the immune response to elicit either stronger antibody-mediated immunity or stronger cellular immunity, which has implications in both infectious disease and cancer vaccine applications. Of note, our study utilized a single ionizable lipid for detailed characterization. Another limitation of this study is the absence of LNP groups containing 0.5% PEG with DOPS and 1.5% PEG with DOPG due to the reasons mentioned above. Future research will assess our findings across a broader range of formulations. Testing these LNP formulations in non-human primates will provide further insights.

Online content

Any methods, additional references, Nature Portfolio reporting summaries, source data, extended data, supplementary information, acknowledgements, peer review information; details of author contributions and competing interests; and statements of data and code availability are available at https://doi.org/10.1038/s41565-025-01958-5.

References

1. Hogan, M. J. & Pardi, N. mRNA vaccines in the COVID-19 pandemic and beyond. *Annu. Rev. Med.* **73**, 17–39 (2022).
2. Patel, R., Kaki, M., Potluri, V. S., Kahar, P. & Khanna, D. A comprehensive review of SARS-CoV-2 vaccines: Pfizer, Moderna & Johnson & Johnson. *Hum. Vaccines Immunother.* **18**, 2002083 (2022).
3. Polack, F. P. et al. Safety and efficacy of the BNT162b2 mRNA Covid-19 vaccine. *N. Engl. J. Med.* **383**, 2603–2615 (2020).
4. Baden, L. R. et al. Efficacy and safety of the mRNA-1273 SARS-CoV-2 vaccine. *N. Engl. J. Med.* **384**, 403–416 (2021).
5. Author(s) et al. *COMIRNATY—COVID-19 Vaccine, mRNA Injection, Suspension [Package Insert]* Report No. xxxx (Pfizer Laboratories Div Pfizer Inc., 2023).
6. Author(s) et al. *SPIKEVAX—COVID-19 Vaccine, mRNA Injection, Suspension [Package Insert]* Report No. xxxx (Moderna US, Inc., 2023).
7. Karikó, K., Buckstein, M., Ni, H. & Weissman, D. Suppression of RNA recognition by toll-like receptors: the impact of nucleoside modification and the evolutionary origin of RNA. *Immunity* **23**, 165–175 (2005).
8. Karikó, K. et al. Incorporation of pseudouridine into mRNA yields superior nonimmunogenic vector with increased translational capacity and biological stability. *Mol. Ther.* **16**, 1833–1840 (2008).
9. Pardi, N. et al. Expression kinetics of nucleoside-modified mRNA delivered in lipid nanoparticles to mice by various routes. *J. Control. Release* **217**, 345–351 (2015).
10. Alameh, M.-G. et al. Lipid nanoparticles enhance the efficacy of mRNA and protein subunit vaccines by inducing robust T follicular helper cell and humoral responses. *Immunity* **54**, 2877–2892.e7 (2021).
11. Tahtinen, S. et al. IL-1 and IL-1ra are key regulators of the inflammatory response to RNA vaccines. *Nat. Immunol.* **23**, 532–542 (2022).
12. Cullis, P. R. & Hope, M. J. Lipid nanoparticle systems for enabling gene therapies. *Mol. Ther.* **25**, 1467–1475 (2017).
13. Hald Albertsen, C. et al. The role of lipid components in lipid nanoparticles for vaccines and gene therapy. *Adv. Drug Deliv. Rev.* **188**, 114416 (2022).
14. Dilliard, S. A. & Siegwart, D. J. Passive, active and endogenous organ-targeted lipid and polymer nanoparticles for delivery of genetic drugs. *Nat. Rev. Mater.* **8**, 282–300 (2023).

15. Cheng, Q. et al. Selective organ targeting (SORT) nanoparticles for tissue-specific mRNA delivery and CRISPR–Cas gene editing. *Nat. Nanotechnol.* **15**, 313–320 (2020).
16. LoPresti, S. T., Arral, M. L., Chaudhary, N. & Whitehead, K. A. The replacement of helper lipids with charged alternatives in lipid nanoparticles facilitates targeted mRNA delivery to the spleen and lungs. *J. Control. Release* **345**, 819–831 (2022).
17. Hassett, K. J. et al. Optimization of lipid nanoparticles for intramuscular administration of mRNA vaccines. *Mol. Ther. Nucleic Acids* **15**, 1–11 (2019).
18. Han, X. et al. Adjuvant lipidoid-substituted lipid nanoparticles augment the immunogenicity of SARS-CoV-2 mRNA vaccines. *Nat. Nanotechnol.* **18**, 1105–1114 (2023).
19. Lokugamage, M. P. et al. Optimization of lipid nanoparticles for the delivery of nebulized therapeutic mRNA to the lungs. *Nat. Biomed. Eng.* **5**, 1059–1068 (2021).
20. Chander, N., Basha, G., Cheng, M. H. Y., Witzigmann, D. & Cullis, P. R. Lipid nanoparticle mRNA systems containing high levels of sphingomyelin engender higher protein expression in hepatic and extra-hepatic tissues. *Mol. Ther. Methods Clin. Dev.* **30**, 235–245 (2023).
21. Tang, X. et al. Simultaneous dendritic cells targeting and effective endosomal escape enhance sialic acid-modified mRNA vaccine efficacy and reduce side effects. *J. Control. Release* **364**, 529–545 (2023).
22. Kim, J. et al. Engineering lipid nanoparticles for enhanced intracellular delivery of mRNA through inhalation. *ACS Nano* **16**, 14792–14806 (2022).
23. Zhang, R. et al. Helper lipid structure influences protein adsorption and delivery of lipid nanoparticles to spleen and liver. *Biomater. Sci.* **9**, 1449–1463 (2021).
24. Álvarez-Benedicto, E. et al. Optimization of phospholipid chemistry for improved lipid nanoparticle (LNP) delivery of messenger RNA (mRNA). *Biomater. Sci.* **10**, 549–559 (2022).
25. Lam, K. et al. Unsaturated, trialkyl ionizable lipids are versatile lipid-nanoparticle components for therapeutic and vaccine applications. *Adv. Mater.* **35**, 2209624 (2023).
26. Puthanakit, T. et al. Phase II prefusion non-stabilised Covid-19 mRNA vaccine randomised study. *Sci. Rep.* **14**, 2373 (2024).
27. Hassett, K. J. et al. Impact of lipid nanoparticle size on mRNA vaccine immunogenicity. *J. Control. Release* **335**, 237–246 (2021).
28. Kirchdoerfer, R. N. et al. Pre-fusion structure of a human coronavirus spike protein. *Nature* **531**, 118–121 (2016).
29. Leung, A. K. K., Tam, Y. Y. C., Chen, S., Hafez, I. M. & Cullis, P. R. Microfluidic mixing: a general method for encapsulating macromolecules in lipid nanoparticle systems. *J. Phys. Chem. B* **119**, 8698–8706 (2015).
30. Cheng, M. H. Y. et al. Induction of bleb structures in lipid nanoparticle formulations of mRNA leads to improved transfection potency. *Adv. Mater.* **35**, e2303370 (2023).
31. Mendonça, M. C. P., Kont, A., Kowalski, P. S. & O'Driscoll, C. M. Design of lipid-based nanoparticles for delivery of therapeutic nucleic acids. *Drug Discov. Today* **28**, 103505 (2023).
32. Li, J. et al. A review on phospholipids and their main applications in drug delivery systems. *Asian J. Pharm. Sci.* **10**, 81–98 (2015).
33. Sallusto, F., Lanzavecchia, A., Araki, K. & Ahmed, R. From vaccines to memory and back. *Immunity* **33**, 451–463 (2010).
34. Laczkó, D. et al. A single immunization with nucleoside-modified mRNA vaccines elicits strong cellular and humoral immune responses against SARS-CoV-2 in mice. *Immunity* **53**, 724–732.e7 (2020).
35. Verma, C. et al. Cancer vaccines in the immunotherapy era: promise and potential. *Vaccines* **11**, 1783 (2023).
36. Tallón de Lara, P., Castañón, H., Sterpi, M. & van den Broek, M. Antimetastatic defense by CD8+ T cells. *Trends Cancer* **8**, 145–157 (2022).
37. Johansen, P. et al. Antigen kinetics determines immune reactivity. *Proc. Natl Acad. Sci. USA* **105**, 5189–5194 (2008).
38. Dilliard, S. A., Cheng, Q. & Siegwart, D. J. On the mechanism of tissue-specific mRNA delivery by selective organ targeting nanoparticles. *Proc. Natl Acad. Sci. USA* **118**, e2109256118 (2021).
39. Akinc, A. et al. Targeted delivery of RNAi therapeutics with endogenous and exogenous ligand-based mechanisms. *Mol. Ther.* **18**, 1357–1364 (2010).
40. Kulkarni, J. A., Cullis, P. R. & van der Meel, R. Lipid nanoparticles enabling gene therapies: from concepts to clinical utility. *Nucleic Acid Ther.* **28**, 146–157 (2018).
41. Bettini, E. et al. Distinct components of nucleoside-modified messenger RNA vaccines cooperate to instruct efficient germinal center responses. Preprint at *bioRxiv* https://doi.org/10.1101/2024.05.17.594726 (2024).
42. Yang, L. et al. Recent advances in lipid nanoparticles for delivery of mRNA. *Pharmaceutics* **14**, 2682 (2022).
43. Remaut, K., Lucas, B., Braeckmans, K., Demeester, J. & De Smedt, S. C. Pegylation of liposomes favours the endosomal degradation of the delivered phosphodiester oligonucleotides. *J. Control. Release* **117**, 256–266 (2007).
44. Tanaka, H. et al. Improvement of mRNA delivery efficiency to a T cell line by modulating PEG-lipid content and phospholipid components of lipid nanoparticles. *Pharmaceutics* **13**, 2097 (2021).
45. Huang, Y., Jia, A., Wang, Y. & Liu, G. $CD8^+$ T cell exhaustion in anti-tumour immunity: the new insights for cancer immunotherapy. *Immunology* **168**, 30–48 (2023).
46. Zhu, Y. et al. Screening for lipid nanoparticles that modulate the immune activity of helper T cells towards enhanced antitumour activity. *Nat. Biomed. Eng.* **8**, 544–560 (2024).
47. Bevers, S. et al. mRNA-LNP vaccines tuned for systemic immunization induce strong antitumor immunity by engaging splenic immune cells. *Mol. Ther.* **30**, 3078–3094 (2022).
48. Luozhong, S. et al. Phosphatidylserine lipid nanoparticles promote systemic RNA delivery to secondary lymphoid organs. *Nano Lett.* **22**, 8304–8311 (2022).
49. Gomi, M. et al. Delivering mRNA to secondary lymphoid tissues by phosphatidylserine-loaded lipid nanoparticles. *Adv. Healthc. Mater.* **12**, e2202528 (2023).
50. Ben-Sasson, S. Z. et al. IL-1 enhances expansion, effector function, tissue localization, and memory response of antigen-specific CD8 T cells. *J. Exp. Med.* **210**, 491–502 (2013).
51. Van Den Eeckhout, B. et al. Specific targeting of IL-1β activity to $CD8^+$ T cells allows for safe use as a vaccine adjuvant. *npj Vaccines* **5**, 64 (2020).
52. Ghiringhelli, F. et al. Activation of the NLRP3 inflammasome in dendritic cells induces IL-1beta-dependent adaptive immunity against tumors. *Nat. Med.* **15**, 1170–1178 (2009).

[1]Department of Microbiology, Perelman School of Medicine, University of Pennsylvania, Philadelphia, PA, USA. [2]Genevant Sciences Corporation, Vancouver, British Columbia, Canada. [3]Department of Molecular and Medical Pharmacology, David Geffen School of Medicine, University of California, Los Angeles, CA, USA. [4]The Department of Pathology and Laboratory Medicine, Perelman School of Medicine, University of Pennsylvania, Philadelphia, PA, USA. [5]Department of Systems Pharmacology and Translational Therapeutics, Perelman School of Medicine, University of Pennsylvania, Philadelphia, PA, USA. [6]Department of Bioengineering, University of Pennsylvania, Philadelphia, PA, USA. [7]Institute for Immunology and Immune Health, Perelman School of Medicine, University of Pennsylvania, Philadelphia, PA, USA. [8]Synthetic and Systems Biology Unit, Institute of Biochemistry, HUN-REN Biological Research Centre, Szeged, Hungary. [9]National Laboratory for Biotechnology, Institute of Genetics, HUN-REN Biological Research Centre, Szeged, Hungary. [10]Present address: Key Laboratory of RNA Innovation, Science and Engineering, CAS Center for Excellence in Molecular Cell Science, Shanghai Institute of Biochemistry and Cell Biology, Chinese Academy of Sciences, University of Chinese Academy of Sciences, Shanghai, China. [11]These authors contributed equally: Máté Vadovics, Wenchen Zhao, Emily F. Daley. ✉e-mail: pnorbert@pennmedicine.upenn.edu

Methods

Ethics statement

This study was performed in collaboration with researchers from multiple institutions, ensuring equitable contribution and authorship. All collaborators were involved in the study design, data analysis and manuscript preparation. In this study, peripheral blood mononuclear cells (PBMCs) were isolated from the blood of healthy donors and used to generate HuMDDCs. All participants were recruited through the University of Pennsylvania Human Immunology Core (SCR_022380) and provided written informed consent. The investigators faithfully adhered to the 'Guide for the Care and Use of Laboratory Animals' by the Committee on Care of Laboratory Animal Resources Commission on Life Sciences, National Research Council. Mouse studies were conducted under protocols approved by the Institutional Animal Care and Use Committees of the University of Pennsylvania (IACUC 807165), the University of California (C-07-149) and Genevant Sciences Corporation (AUP 0722001). All animals were housed and cared for according to local, state and federal policies in a facility accredited by the Association for Assessment and Accreditation of Laboratory Animal Care International.

Mice

BALB/c mice aged 8 weeks were purchased from Charles River Laboratories. Female C57BL/6J (Jackson Laboratory strain no. 000664) and Pmel-1 TCR/Thy1.1 transgenic mice (Jackson Laboratory strain no. 005023) on a C57BL/6 background (aged 6–8 weeks) were purchased from the Jackson Laboratory. Pmel-1 mice were bred and maintained at the University of California, Los Angeles, breeding vivarium and utilized for experiments when reaching 8–12 weeks of age.

Mice were housed under a 12-h light/12-h dark cycle at 22 °C ± 2 °C with a humidity of 50 ± 20%. Food and water were available ad libitum.

Cell

Murine DC2.4 cell line was obtained from Millipore Sigma (no. SCC142M) and maintained in Dulbecco's modified Eagle's medium (Corning, no. 10-013-CV) supplemented with 10% foetal bovine serum (FBS; Cytivia Hyclone, no. SH30071.03) and 100 U ml^{-1} penicillin–streptomycin (Gibco. no. 15140-122).

HuMDDCs were generated from a healthy donor apheresis product, provided by the University of Pennsylvania Human Immunology Core. Dendritic cells were derived from monocytes using complete Roswell Park Memorial Institute (RPMI) media (Gibco, no. 22400-089) supplemented with human granulocyte colony-stimulating factor (R&D Systems, no. 215GM010CF) and human IL-4 (R&D Systems, no. 204IL010CF). Expi293F cells were obtained from Thermo Fisher Scientific (no. A14527) and maintained in Expi293 Expression Medium (Thermo Fisher Scientific, no. A1435101). Sf9 cells were obtained from Thermo Fisher Scientific (no. 12659017) and maintained in Sf-900 III SFM, a serum-free medium (Thermo Fisher Scientific, no. 12658019), supplemented with 1× penicillin–streptomycin (Capricorn, 100× stock solution). High Five cells were obtained from Thermo Fisher Scientific (no. B85502) and maintained in HyClone SFX-Insect liquid medium (Cytiva, no. SH30278.LS). 293T cells were obtained from the American Type Culture Collection (no. CRL-3216) and maintained in Dulbecco's modified Eagle's medium (Life Technologies, no. 11995065) supplemented with 10% FBS (Hyclone, no. SH30071.03). Vero E6-TMPRSS2 cells were generated in-house, selected once with blasticidin (no. R21001) and maintained in Dulbecco's modified Eagle's medium (Life Technologies, no. 11995065).

mRNA–LNP vaccine production

mRNA vaccines were designed based on the S-2P sequence (Wuhan-Hu-1, GenBank: MN908947.3); the HA sequence from A/Puerto Rico/8/1934 (H1N1); or the melanoma-associated antigen, gp100.

The HA mRNA was produced at Genevant. Briefly, the codon-optimized HA sequence was synthesized (GenScript) and cloned into the mRNA production plasmid. HA mRNA was produced using T7 RNA polymerase (MEGAscript, Ambion) on linearized plasmids. The HA mRNA was then enzymatically polyadenylated (NEB). Pseudouridine-5′-triphosphate (TriLink) was used instead of uridine 5′-triphosphate to generate HA with modified nucleoside-containing mRNA. Capping of the in vitro-transcribed mRNA was performed co-transcriptionally using the trinucleotide cap1 analogue, CleanCap (TriLink). mRNA was purified by cellulose purification[53].

To produce the S-2P, Luc, eGFP and gp100 mRNAs, the sequences were codon optimized, synthesized and cloned into an mRNA production plasmid[54,55]. N1-methylpseudouridine-5′-triphosphate (m1Ψ-5′-triphosphate; TriLink no. N-1081) instead of uridine 5′-triphosphate was used to generate the modified nucleoside-containing mRNAs, and the mRNAs were transcribed to have 101-nucleotide-long poly(A) tails. Co-transcriptional capping of the in vitro-transcribed mRNAs was performed using the trinucleotide cap1 analogue, CleanCap (TriLink no. N-7413). Cellulose (Sigma-Aldrich no. 11363-250G) was used for mRNA purification[53,54]. All mRNAs were evaluated by agarose gel electrophoresis and were stored frozen at −20 °C.

Cellulose-purified S-2P, HA, Luc, eGFP and gp100 mRNAs were encapsulated by a controlled mixing, self-assembly process. An ethanolic lipid mixture of ionizable lipid (6Z,16Z)-12-((Z)-dec-4-en-1-yl) docosa-6,16-dien-11-yl 5-(dimethylamino) pentanoate (3D-P-DMA), phospholipid, cholesterol and PEG lipid[56] was mixed with an aqueous solution containing mRNA at an acidic pH of 5. Post-formation, the ethanol was removed from the LNP via dialysis with 10,000-molecular-weight-cut-off Thermo Fisher Slide-a-Lyzer cassettes (A52973), concentrated with a Vivaspin (10,000 molecular weight cut-off; Cytiva, no. 28932363), and further dialysed into Tris-sucrose buffer at pH 8. Samples were sterile filtered, characterized, adjusted to approximately 0.5 mg ml^{-1} of total mRNA and frozen at −80 °C. The ionizable and PEG-conjugated lipids were synthesized at Genevant. Cholesterol was obtained from Sigma-Aldrich (Synthechol, no. W004591) and the phospholipids from Avanti Polar Lipids via Millipore Sigma (DSPC no. 730365, DOPS no. 840035P and DOPG no. 840475). LNP for in vitro and in vivo uptake assays were prepared as above with the addition of 1% of 1,1′-dioctadecyl-3,3,3′,3′-tetramethylindocarbocyanine (DiI; Millipore Sigma, no. 42364) fluorescent lipid in the lipid stock.

Recombinant protein production

RBD. The DNA sequences encoding the signal peptide (amino acids 1–14) and the RBD (amino acids 319–541) of SARS-CoV-2 spike surface glycoprotein (NCBI reference sequence: YP_009724390) in fusion with a C-terminal hexahistidine affinity-tag (His6, GHHHHHH) and a stop codon (hereafter referred to as RBD) were optimized to the mammalian codon preference, produced by gene synthesis (GenScript), and sub-cloned into the pCDNA3.1(−) mammalian expression plasmid (no. V79520, Thermo Fisher Scientific). Recombinant RBD was produced in Expi293F mammalian cells and affinity purified from a cell culture supernatant following the protocol described in detail in our prior study[57]. Purified RBD was buffer exchanged to phosphate-buffered saline (PBS) and concentrated to 1 mg ml^{-1} using an Amicon Ultra centrifugal filter unit (molecular weight cut-off = 10 kDa; no. UFC9010, Merck Millipore), sterile filtered and flash frozen in liquid nitrogen. The integrity and purity of the proteins were tested by reducing and non-reducing sodium dodecyl sulfate–polyacrylamide gel electrophoresis and western blotting techniques[57].

HA. Soluble and homotrimeric recombinant HA was synthesized in insect cells using a modified protocol described previously[41,58]. The DNA sequence encompassing the signal peptide (amino acids 1–17) and the ectodomain (amino acids 18–529) of the HA of the influenza A virus (A/Puerto Rico/8/1934 (PR8); GenBank: ADX99484.1) in fusion with the thrombin cleavage site (RS*LVPRGSP*), followed by the foldon trimerization domain of the T4 bacteriophage fibritin

(*GSGYIPEAPRDGQAYVRKDGEWVLLSTFL*, according to refs. 59,60 and a C-terminal hexahistidine affinity-tag and stop codon was produced by gene synthesis (GenScript), and sub-cloned into the pFastBac-HTA vector (no. 10584027, Thermo Fisher Scientific)). Bacmids were created in DH10Bac *Escherichia coli* cells, whereas recombinant baculovirus stocks (p1, p2 and p3) were generated and produced in *Spodoptera frugiperda* Sf9 insect cells at 27 °C in Sf-900 III serum-free medium following the guidelines of the Bac-to-Bac Baculovirus Expression System manual (no. 10359016, Thermo Fisher Scientific). Recombinant HA was expressed in *Trichoplusia ni* High Five insect cells cultured in HyClone SFX-Insect medium (no. SH30278.LS, Cytiva) as follows: High Five cells from six confluent T175 flasks were harvested, collected by centrifugation (1,200*g*, 24 °C, 10 min) and mixed with 15 ml of p3 baculovirus stock. The mixture was incubated at room temperature (RT) for 20 min and added to 210 ml of HyClone SFX-Insect medium in 1 l of PETG tissue culture Erlenmeyer flasks (no. 4115-1000, Nalgene). The cells were grown at 28 °C on a shaker at 75 rpm for 72 h. The cell culture supernatant, containing the secreted homotrimeric HA protein, was collected by centrifugation (2,000*g*, 4 °C, 10 min), filtered and subjected to affinity purification following the steps outlined in the above detailed RBD purification protocol[57]. The purified HA was buffer exchanged to PBS, concentrated to 1 mg ml^{-1}, sterile filtered and flash frozen in liquid nitrogen. The integrity and purity of HA were assessed using reducing and non-reducing sodium dodecyl sulfate–polyacrylamide gel electrophoresis and western blotting techniques.

Mouse immunizations

mRNA formulated into the LNP compositions were diluted in PBS and injected into the gastrocnemius muscle (40 µl of injection volume) with a 3/10 ml 29½ G insulin syringe (Covidien, no. 8881600145).

Blood collection

Blood was collected from the orbital sinus under isoflurane anaesthesia. Blood was centrifuged for 5 min at 13,000*g*, and the serum was stored at −20 °C and used for further analysis.

End-point ELISA

RBD-specific ELISA: in Corning 96-Well EIA/RIA Clear Flat-Bottom Polystyrene High-Bind Microplates (Corning no. 3590), 1 µg ml^{-1} of purified RBD in PBS (100 µl per well) was added overnight at 4 °C for protein coating. The following day, the coated plates were washed four times with a wash buffer (0.05% Tween-20 in PBS). The plates were then blocked with 2% bovine serum albumin (BSA) in PBS for 2 h at RT and washed three times with the wash buffer. Mouse sera were diluted in the blocking buffer and incubated for 2 h at RT, followed by three washes. HRP-conjugated anti-mouse secondary antibody (total IgG, Jackson Immunoresearch no. 115-035-003; IgG1, polyclonal, abcam, no. AB98693; IgG2a, polyclonal, abcam, no. AB98698; IgG2b, polyclonal, abcam, no. AB98703; IgA, polyclonal, abcam, no. AB97235) was diluted 1:10,000 (IgA, 1:5,000) in the blocking buffer and incubated for 1 h, followed by three washes. KPL two-component TMB Microwell Peroxidase Substrate (Seracare no. 5120-0047) was applied to the plate and the reaction was stopped with 2-N sulfuric acid. Using a SpectraMax 190 microplate reader, the absorbance was measured at 450 nm. A cut-off value of the average of the optical density values of blank wells plus three standard deviations was determined for each plate and used for calculating the area under the curve (AUC). The limit of detection of the assay was a titre of 1:100.

SARS-CoV-2 neutralization assay

Production of VSV pseudotypes with SARS-CoV-2 spike:293T cells were plated at 3.5×10^6 cells per 10 cm dish; 24 h later, they were transfected using calcium phosphate with 25 µg of pCG1 SARS-CoV-2 Spike D614G delta18 expression plasmid encoding a codon-optimized SARS-CoV2 Spike gene with an 18-residue truncation in the cytoplasmic tail. Twelve hours after transfection, the cells were fed with fresh media containing 5 mM of sodium butyrate to increase the expression of the transfected DNA. Thirty hours post-transfection, the SARS-CoV-2 spike-expressing cells were infected for 2–4 h with VSV-G pseudotyped VSVΔG-RFP at a multiplicity of infection of ~3–5. Following infection, the cells were washed twice with media to remove the unbound virus. Media containing the VSVΔG-RFP SARS-CoV-2 pseudotypes were harvested 28–30 h after infection and clarified by centrifugation twice at 1,250*g* and then aliquoted and stored at −80 °C until used for antibody neutralization analysis.

Antibody neutralization assay using VSVΔG-RFP SARS-CoV-2: all sera were heat inactivated for 30 min at 55 °C before use in the neutralization assay. In a 96-well collagen-coated plate, Vero E6 cells stably expressing TMPRSS2 were seeded in 100 µl at 2.5×10^4 cells per well. The next day, twofold serially diluted serum samples were mixed with VSVΔG-RFP SARS-CoV-2 pseudotype virus (100–300 focus-forming units per well) and incubated for 1 h at 37 °C. To neutralize any potential VSV-G carryover virus, this mixture also included 1E9F9, a mouse anti-VSV Indiana G, at a concentration of 600 ng ml^{-1} (Absolute Antibody, no. Ab01402-2.0). The media on Vero E6-TMPRSS2 cells were then replaced with the serum-virus mixture. After 22 h of infection, the cells were washed and fixed with 4% paraformaldehyde before visualization on an S6 FluoroSpot Analyser (CTL, Shaker Heights). Individual infected foci were quantified and the values were compared with control wells without antibody. Focus reduction neutralization titre 50% ($FRNT_{50}$) was measured as the greatest serum dilution at which the focus count was reduced by at least 50% relative to the control cells that were infected with the pseudotype virus in the absence of mouse serum. $FRNT_{50}$ titres for each sample were measured in at least two technical replicates and were reported for each sample as the geometric mean.

Flow cytometry analysis of MBCs/LLPCs in mouse splenocytes and bone marrow

Splenocytes were harvested from spleens by mechanical disruption between frosted slides and filtered through a 63-µm Nitex mesh. Bone marrow was flushed from the femurs and tibia from each mouse using a 23 G × ¾″ needle and syringe into FACS buffer (PBS + 2% FBS) and filtered through a 63-µm Nitex mesh. Red blood cells were lysed with ammonium–chloride–potassium (ACK) lysis buffer (Lonza, no. 10-548E) for 5 min on ice and the reaction was stopped with ten times the volume of PBS. Five million cells were then stained with fixable live–dead aqua (BioLegend Zombie Aqua, 423101; 1:500 in PBS) for 15 min at RT. Cells were then washed with FACS buffer and stained with the respective dilutions of antibodies (Supplementary Table 4) in BD Brilliant Staining Buffer (BD Biosciences, no. 563794) for 15 min at 4 °C. To create fluorescently labelled RBD tetramers, recombinant RBD was biotinylated using the EZ-Link Micro Sulfo-NHS-Biotinylation Kit (Thermo Fisher). Streptavidin-conjugated Alexa PE and Alexa Flour 647 (all from BioLegend) were then added at a 6:1 molar ratio (biotinylated protein to streptavidin conjugate). Specifically, after the volume of fluorochrome needed to achieve a 6:1 molar ratio was determined, the total volume of fluorochrome was split into ten subaliquots. These subaliquots were then added, on ice, to the biotinylated protein and mixed by pipetting every 10 min (for a total of 10 additions). Here 2.5 million events per sample were acquired on a BD Symphony A3 Lite and analysed with FlowJo v. 10 software. The gating strategy is provided in Supplementary Fig. 5.

ELISpot assay

Bone marrow was flushed from the femurs and tibia from each mouse using a 23 G × ¾″ needle and syringe into FACS buffer and filtered through a 63-µm Nitex mesh. Red blood cells were lysed with ACK lysis buffer (Lonza, no. 10-548E) for 5 min on ice and the reaction was stopped with ten times the volume of PBS. The resulting cells were

counted using a Cellaca MX cell counter (Nexcelom Bioscience). MultiScreenHTS IP Filter Plate 0.45 µm (Millipore Sigma, no. MSIPS4W10) were coated with recombinant RBD protein at 5 µg ml^{-1} in sodium carbonate/ sodium bicarbonate buffer at pH 9.6 (35 mM of $NaHCO_3$ and 15 mM of Na_2CO_3) for 1 h at 37 °C. Plates were then washed with 200 µl of PBS per well three times and blocked at 37 °C in complete RPMI + 10% FBS for 30 min. Bone marrow cells were plated in six halving dilutions beginning with one million total bone marrow cells per well and incubated overnight in complete RPMI + 10% FBS. Plates were then washed with a wash buffer (1× PBS + 0.1% Tween-20) five times and incubated with various biotinylated anti-IgG detection antibodies (Supplementary Table 5) in PBS + 2% BSA at RT for 1 h. Plates were once again washed five times, and streptavidin–alkaline phosphatase (1:20,000 dilution in PBS + 2% BSA) was added before incubation at RT for 30 min. Plates were then washed five times with the wash buffer, and 50 µl per well of BCIP/NBT single solution (Sigma, no. B1911-100ml) was added for approximately 5 min or until spots developed, at which time the reaction was quenched with 100 µl of 1-M sodium phosphate monobasic solution. After the plates were rinsed with distilled water and dried overnight, they were scanned and counted using CTL ImmunoSpot hardware and software (ImmunoSpot).

Spike-specific CD4$^+$ and CD8$^+$ T cell studies

BALB/c mice received a single i.m. immunization with 5 µg of S-2P mRNA encapsulated in different LNP formulations. Splenocytes were collected from animals 10 days after injection. Sample processing: spleens were mashed in complete RPMI 1640 medium (American Type Culture Collection modification; Gibco, no. A1049101) on ice and filtered through a 40-µm cell strainer. Red blood cells were lysed with ACK lysis buffer (Lonza, no. 10-548E) for 5 min on ice and the reaction was stopped with ten times the volume of PBS. Then, 1×10^6 cells per sample were stimulated for 11 h at 37 °C and 5% CO_2, in the presence of SARS-CoV-2 Spike Glycoprotein peptide pool (JPT Peptide Technologies, no. PM-WCPV-S-2) at 1.8 µg ml^{-1} per peptide. GolgiPlug (1:250; brefeldin A; BD Biosciences, no. 51-2301KZ) and GolgiStop (1:250; monensin; BD Biosciences, no. 51-2092KZ) were added to each sample 1 h after the start of the stimulation. Unstimulated samples for each animal were included. A sample stimulated with phorbol 12-myristate-13-acetate (25 ng ml^{-1}; Sigma, no. P1585) and ionomycin (2.5 µg ml^{-1}; Sigma, no. 13909) was included as a positive control. After stimulation, cells were washed with PBS and stained for 10 min in the dark at 25 °C with the LIVE/DEAD Fixable Aqua Dead Cell Stain Kit (1:60, Life Technologies, no. L34957). Samples were incubated in Fc blocker (1:25, Purified Rat Anti-Mouse CD16/CD32, BD Biosciences, clone 2.4G2, no. 553142) for 10 min in the dark at 4 °C and then surface stained with the monoclonal antibodies anti-CD4 PerCP/Cy5.5 (1:100, clone GK1.5, BioLegend, no. 100434) and anti-CD8 Pacific Blue (1:100, clone 53-6.7, BioLegend, no. 100725) for 30 min at 4 °C. After surface staining, cells were washed with FACS buffer, fixed and permeabilized using the Cytofix/Cytoperm kit (BD Biosciences, no. 51-2090KZ), and washed again using the permeabilization buffer (BD Biosciences, no. 51-2091KZ). Cells were intracellularly stained with anti-CD3 APC-Cy7 (1:50, clone, 145-2C11, BD Biosciences, no. 561042), anti-TNF-α PE-Cy7 (1:50, clone MP6-XT22, BD Biosciences, no. 557644) and anti-IFN-γ AF700 (1:50, clone XMG1.2, BD Biosciences, no. 557998) monoclonal antibodies for 30 min at 4 °C. Next, the cells were washed twice with the permeabilization buffer (BD Biosciences, no. 51-2091KZ) and once with FACS buffer, fixed with 4% paraformaldehyde in PBS and stored at 4 °C until analysis. Splenocytes were analysed on an LSR II flow cytometer (BD Biosciences). Overall, 200,000 events were collected per specimen. Data were analysed using FlowJo v. 100. Data were expressed by subtracting the percentages of the unstimulated stained cells from the percentages of the peptide-pool-stimulated stained samples. Any value less than zero is represented as zero. The gating strategy is provided in Supplementary Fig. 6.

gp100-specific CD8$^+$ T cell studies

Thy1.1$^+$ CD8$^+$ T cells were purified from the spleens of female Pmel-1 mice by negative selection using the EasySep Mouse CD8$^+$ T cell Isolation Kit (Stem Cell Technologies, no. 19853) according to the manufacturer's protocol. Enriched pmel-1 CD8$^+$ T cells were washed three times with sterile 1× PBS. A physiological precursor frequency number of cells (5×10^3 to 7×10^3) was transferred to each naive, lymphoreplete recipient female C57BL/6 mouse through a tail-vein injection (200 µl per injection). Mice were subsequently immunized with either a 1-µg prime and 1-µg boost (bolus immunization) or four equal 1.25-µg injections (extended prime immunization) of mRNA–LNP encoding murine full-length gp100 and the modified peptide sequence (EGPRNQDWL). Negative control mice were injected with the same doses of mRNA–LNP encoding firefly luciferase as an irrelevant antigen (Luc mRNA–LNP). Flow cytometric analysis of the circulating antigen-specific CD8$^+$ T cells in the peripheral blood was performed 5–6 days after the last immunization. Peripheral blood was obtained from mice through retro-orbital eye bleeds under anaesthesia and collected into 1.5-ml Eppendorf tubes containing 2 µl of 0.5-M EDTA to inhibit coagulation. Blood samples were subjected to three cycles of red blood cell lysis using 500 µl of ACK lysis buffer each cycle. Samples were resuspended in FACS buffer (1× PBS containing 5% FBS and 2 mM of EDTA), passed through a 70-µm filter to remove debris, counted and finally allocated for downstream flow cytometric analyses or functional assays.

For intracellular cytokine staining and flow cytometry analyses, PBMCs were plated at 1×10^5 cells per well in a 96-well round-bottom plate and restimulated for 5 h with the murine gp10025-33 epitope (EGSRNQDWL) peptide at 1 µg ml^{-1} in complete RPMI 1640 medium (supplemented with 10% FBS, 1% penicillin–streptomycin and 55 µM of β-mercaptoethanol) at 37 °C in the presence of brefeldin A (15 µg ml^{-1}). After 5 h, cells were collected and stained with Fixable Viability Dye eFluor 780 stainings (1:1,000, Thermo Fisher Scientific, no. 65-0865) or Zombie Violet Fixable Viability dye (1:200, BioLegend, no. 423114) for 15–30 min on ice in 1× PBS. After washing out the viability dye, cells were stained for cell surface markers in FACS buffer. Intracellular staining of the cytokines was performed using the Cyto-Fast Fix/Perm Buffer Set (BioLegend, no. 426803) according to the manufacturer's protocol. Cell surface antibodies include anti-CD3 on PerCP/cyanine5.5 (1:100, BioLegend, no. 100218, clone 17A2) or APC (1:100, BioLegend, no. 100312, clone 145-2C11), anti-CD8 on PE/cyanine7 (1:200, BioLegend, no. 100722, clone 53-6.7), anti-CD90.1 (Thy1.1) on FITC (1:400, BioLegend, no. 202504, clone OX-7), anti-KLRG1 on PE (1:200, BioLegend, no. 138408, clone 2F1/KLRG1) and anti-CD127 (IL-7Rα) on APC/cyanine7 (1:100, BioLegend, no. 135040, clone A7R34). Cytokine antibodies include anti-IFN-γ on PE (1:100, BioLegend, no. 505808, clone XMG1.2) or Brilliant Violet 421 (1:100, BioLegend, no. 505830, clone XMG1.2), anti-TNF-α on Brilliant Violet 711 (1:100, BioLegend, no. 506349, clone MP6-XT22). Following the completion of antibody staining, cells were treated with 1.6% methanol-free formaldehyde and resuspended in 1× PBS. Sample data were acquired on the Thermo Fisher Scientific NxT Attune flow cytometer in the University of California, Los Angeles, Johnson Comprehensive Cancer Center Flow Cytometry Core Laboratory. Samples were compensated using single-stain controls generated using UltraComp eBeads Plus Compensation beads (Invitrogen, no. 01333342). Data were analysed using FlowJo software (v. 10.10.0). The gating strategy is provided in Supplementary Fig. 8.

In vivo bioluminescence imaging studies

Here 3 µg of Luc mRNA formulated in the four LNP compositions was diluted in PBS and injected into the gastrocnemius muscle (40 µl of injection volume) with a 3/10 ml 29½ G insulin syringe (Covidien, no. 8881600145). Bioluminescence imaging was performed with an IVIS Spectrum imaging system (Caliper Life Sciences), and data were collected and analysed using Living Image Software v. 4.7.4 (Caliper).

Mice were administered D-luciferin (Regis Technologies, no. RG-1-360242-200) at a dose of 150 mg kg^{-1} intraperitoneally. Mice were anaesthetized after receiving D-luciferin in a chamber with 3% isoflurane (Piramal Healthcare Limited) and placed on the imaging platform and maintained on 2% isoflurane via a nose cone. Mice were imaged at 5 min post-administration of D-luciferin using an exposure time of 5 s or longer to ensure that the acquired signal was within the effective detection range (above noise levels and below charge-coupled device saturation limit). Bioluminescence values were quantified by measuring the photon flux (photons per second) in the region of interest, where the bioluminescence signal emanated using the Living Image Software provided by Caliper.

Luciferase expression in different organs

Here 5 µg of Luc mRNA formulated in the four LNP compositions was diluted in PBS and injected into the gastrocnemius muscle (40 µl of injection volume) with a 3/10 ml 29½ G insulin syringe (Covidien, no. 8881600145). Spleen, draining popliteal and inguinal lymph nodes, and liver were harvested and analysed. Tissues were homogenized in a cell lysis buffer (Promega Corp, no. E1531) using PowerLyzer 24 (Qiagen), received three freeze–thaw cycles and centrifuged for 10 min at 16,000*g* and 4 °C (ref. 61). Luciferase activity of the supernatant was measured using the Luciferase Assay System (Promega, no. E1501) on a Victor3 1420 Multilabel Plate Counter (PerkinElmer). Luciferase activity was normalized by supernatant total protein determined by Lowry assay (DC Protein Assay; BioRad, no. 500-0116) using BSA as a standard and expressed as kLU per mg of protein.

mRNA QuantiGene analysis within different organs

Here 5 µg of Luc mRNA formulated in the four LNP compositions was diluted in PBS and injected into the gastrocnemius muscle (40 µl of injection volume) with a 3/10 ml 29½ G insulin syringe (Covidien, no. 8881600145). Spleen and liver were harvested and analysed. QuantiGene assays were conducted according to the manufacturer's instructions (Thermo Fisher, no. QS0016) using custom-designed probes against luciferase mRNA. Unformulated mRNA was used to prepare the standard curve for quantitation.

3D-P-DMA (ionizable lipid) liquid chromatography/mass spectrometry analysis

Here 5 µg of Luc mRNA formulated in the four LNP compositions was diluted in PBS and injected into the gastrocnemius muscle (40 µl of injection volume) with a 3/10 ml 29½ G insulin syringe (Covidien, no. 8881600145). Spleen and liver tissues were homogenized in PBS buffer using a FastPrep machine for 3 cycles of 5 m s^{-1} × 15 s. Homogenates from the PBS-treated control animals were pooled and used for standard curve preparation. The samples were extracted into a deep-well plate with 160 µl of an internal suitability standard. Plates were stored at −20 °C for 15 min and then centrifuged for 15 min at 4 °C and 500*g*. Analysis was performed using a Q-Exactive Orbitrap MS coupled to a Thermo Vanquish liquid chromatograph, using reverse-phase liquid chromatography separation with an ammonium acetate/isopropanol gradient. Quantitation of the ionizable lipid was by parallel reaction monitoring against a calibration curve. Calibration used a similar class of synthetic lipid as the internal standard.

LNP in vitro cellular uptake study

DC2.4 cells or HuMDDCs were seeded on 35-mm polymer-bottom dishes (Cellvis) overnight using RPMI complete media (RPMI 1640 (Gibco, no. 22400-089), 10% FBS (Cytivia Hyclone, no. SH30071.03), 1% penicillin–streptomycin (Gibco, no. 15140-122)) and then treated with DiI-labelled luciferase mRNA–LNPs at 500 ng ml^{-1} for 2 h. Cells were subsequently washed with PBS and then stained with Hoescht 33342 at 1 ng $µl^{-1}$ for 5 min. Cells were washed with PBS again and covered with RPMI complete media. Images were taken immediately using a confocal laser scanning microscope (LSM 710, ZEISS) at the University of Pennsylvania's Cell & Developmental Biology Microscopy Core. Images were analysed using ImageJ2 (Fiji), an open-source image processing software.

Cell transfections with TransIT-mRNA reagent

DC2.4 cells and HuMDDCs were transfected with mRNA using TransIT-mRNA (Mirus Bio, no. MIR 2225) as per the manufacturer's instructions. mRNA (0.3 µg) was combined with TransIT-mRNA reagent (0.34 µl) and boost reagent (0.22 µl) in 17 µl of serum-free medium, and the complex was added to 6×10^4 cells in 183 µl of complete medium.

Endosomal escape study

DC2.4 cells or HuMDDCs were seeded on eight-well chamber slides (Thermo Fisher Nunc Lab Tek II System) overnight using RPMI complete media (RPMI 1640 (Gibco, no. 22400-089), 10% FBS (Cytivia Hyclone, no. SH30071.03), 1% penicillin–streptomycin (Gibco, no. 15140-122)) and then treated with luciferase mRNA–LNPs at a concentration of 2 µg ml^{-1} for 2 h. Cells were subsequently processed using EEA1/LAMP1 protein staining and luciferase mRNA was tagged with florescence in situ hybridization (RNA FISH) using ViewRNA Cell Plus Assay kit (Thermo Fisher, no. 88-19000-99) following the manufacturer's protocol. In brief, cells were permeabilized/fixed, blocked and incubated with EEA1 and LAMP1 primary antibodies (Thermo Fisher, nos. PA1063A and PA1654A) and a control well with rabbit isotype IgG control (Thermo Fisher, no. 31235) for 1 h at RT at 1:500 dilution in a blocking buffer. For secondary antibodies, the cells were incubated with Alexa Fluor 488 secondary antibody (Thermo Fisher, no. A11070) for 1 h at RT with 1:1,000 dilution. Subsequently, cells were fixed and processed with RNA FISH probes using a custom-designed probe for the luciferase mRNA sequence. GAPDH was also probed as a positive control and dap-B as a negative control. Nuclei were stained with DAPI mountant (Thermo Fisher, no. P36931), and slides were imaged on a CrestOptics X-Light V3 spinning-disc confocal device at the University of Pennsylvania's Cell & Developmental Biology Microscopy Core. Images were analysed using ImageJ2 (Fiji).

Quantification and statistical analysis

Data were collected and expressed as mean ± standard error of the mean (s.e.m.). Data were organized and analysed using Microsoft Excel for Microsoft 365 MSO (v. 2411, build 16.0.18227.20082). Statistical analysis was conducted using GraphPad Prism v. 10.0.0 software package. The significance of the differences between the groups was assessed using the test specified in the legend of the corresponding figure. Differences were considered statistically significant at $P < 0.05$.

Reporting summary

Further information on research design is available in the Nature Portfolio Reporting Summary linked to this article.

Data availability

Source data are provided with this paper. The primary datasets for Supplementary Figs. 1–18, along with detailed results of the statistical analyses, are provided in Supplementary Data 1.

References

53. Baiersdörfer, M. et al. A facile method for the removal of dsRNA contaminant from in vitro-transcribed mRNA. *Mol. Ther. Nucleic Acids* **15**, 26–35 (2019).
54. Vadovics, M., Muramatsu, H., Sárközy, A. & Pardi, N. Production and evaluation of nucleoside-modified mRNA vaccines for infectious diseases. *Methods Mol. Biol.* **2786**, 167–181 (2024).
55. Freyn, A. W. et al. A multi-targeting, nucleoside-modified mRNA influenza virus vaccine provides broad protection in mice. *Mol. Ther.* **28**, 1569–1584 (2020).

56. Heyes, J., Hall, K., Tailor, V., Lenz, R. & MacLachlan, I. Synthesis and characterization of novel poly(ethylene glycol)-lipid conjugates suitable for use in drug delivery. *J. Control. Release* **112**, 280–290 (2006).
57. Ábrahám, E. et al. Expression and purification of the receptor-binding domain of SARS-CoV-2 spike protein in mammalian cells for immunological assays. *FEBS Open Bio* **14**, 380–389 (2024).
58. Margine, I., Palese, P. & Krammer, F. Expression of functional recombinant hemagglutinin and neuraminidase proteins from the novel H7N9 influenza virus using the baculovirus expression system. *J. Vis. Exp.* **81**, e51112 (2013).
59. Stevens, J. et al. Structure of the uncleaved human H1 hemagglutinin from the extinct 1918 influenza virus. *Science* **303**, 1866–1870 (2004).
60. Krammer, F. et al. A carboxy-terminal trimerization domain stabilizes conformational epitopes on the stalk domain of soluble recombinant hemagglutinin substrates. *PLoS ONE* **7**, e43603 (2012).
61. Parhiz, H. et al. PECAM-1 directed re-targeting of exogenous mRNA providing two orders of magnitude enhancement of vascular delivery and expression in lungs independent of apolipoprotein E-mediated uptake. *J. Control. Release* **291**, 106–115 (2018).

Acknowledgements

We thank the Cell & Developmental Biology Microscopy Core at the University of Pennsylvania. Additionally, the flow cytometry data were generated in the Penn Cytomics and Cell Sorting Shared Resource Laboratory at the University of Pennsylvania and is partially supported by a Abramson Cancer Center NCI Grant (P30 016520). The research identifier number is RRid:SCR_022376. The Pardi laboratory was supported by the National Institute of Allergy and Infectious Diseases (NIAID; R01AI146101, R01AI153064, P01AI158571 and U19AI181968). Z.L. was supported by the National Laboratory for Biotechnology (2022-2.1.1-NL-2022-00008) and the Hungarian Academy of Sciences (Lendület Program Grant (LP2017-7/2017)). K.A.L. and P.B. were supported by R01AI 152236. C.G.R. was supported by the NIH-NCI National Cancer Institute; R01CA283736 (C.G.R. and N.P.), the Parker Institute for Cancer Immunotherapy, 20221408 (C.G.R. and N.P.), and the University of California, Los Angeles, Immunology Advisory Committee (IAC) Award (C.G.R.). We also thank Y. Du, H. Sun and E. L. Prak of the Human Immunology Core (HIC) at the Perelman School of Medicine at the University of Pennsylvania for assistance with the Luminex assays, and M. Eldabbas, E. Maddox, T. Sinha and J. Shu for the preparation of deidentified primary human monocytes. The HIC is supported in part by NIH P30 AI045008 and P30 CA016520. HIC RRID: SCR_022380. We also thank M. Katona at the University of Pittsburgh for guidance in confocal imaging quantification methods; L. Palmer, H. Mahmoud, A. Martin, A. Liu and K. McClintock for their contributions and support throughout this project; and the Proteomics Research Group of the HUN-REN BRC Core Facility for performing the liquid chromatography/mass spectrometry analysis and validation of recombinant proteins.

Author contributions

N.P. and J.H. conceived the study. N.P. designed the vaccine antigens. H.M. produced the mRNA vaccine antigens. P.S. encapsulated the mRNAs into LNPs and O.D. performed the immunization studies of PEG lipid titration. M.V. designed, performed and analysed the total IgG ELISA, IVIS and Luminex. K.A.L. and P.B. designed, performed and analysed the FRNT assay. B.T.G., M.V. and D.A. designed, performed and analysed the B cell studies. M.V., E.F.D., K.R., H.R.L. and C.G.R. designed, performed and analysed the T cell studies. M.V., W.Z., K.L., V.V.S., V.R.M., E.Á., G.C., A.H.B., K.N., T.M.L., T.L. and C.G.R. performed, designed and analysed the biodistribution studies. E.F.D., J.X., X.H. and M.J.M. designed, performed and analysed the in vitro LNP uptake studies. E.F.D. performed and analysed the IgG subtypes, IgA ELISA and innate cell infiltration to the injection site studies. E.F.D. and W.Z. designed, performed and analysed the endosomal escape assay. W.Z. performed and analysed the LNP protein corona assay. N.D.L., D.C., E.B. and M.L. designed, performed and analysed the in vivo LNP uptake studies. E.Á. and Z.L. produced the recombinant proteins. A.S. and T.M. helped with the mouse blood collection. M.V., K.L., E.F.D. and N.P. wrote the paper with help from co-authors.

Competing interests

N.P. served on the mRNA strategic advisory board of Sanofi Pasteur in 2022 and Pfizer in 2023–2024. N.P. is also a member of the Scientific Advisory Board of AldexChem and BioNet, and has consulted for Vaccine Company Inc., Optimeos and Pasture Bio. K.L., J.H., O.D., W.Z. and P.S. are employees of Genevant Sciences Corp. and own shares or options of Genevant's parent company. The remaining authors declare no competing interests.

Additional information

Supplementary information The online version contains supplementary material available at https://doi.org/10.1038/s41565-025-01958-5.

Correspondence and requests for materials should be addressed to Norbert Pardi.

Peer review information *Nature Nanotechnology* thanks Roy van der Meel and the other, anonymous, reviewer(s) for their contribution to the peer review of this work.

nature portfolio

Corresponding author(s): Norbert Pardi

Last updated by author(s): Mar 30, 2025

Reporting Summary

Nature Portfolio wishes to improve the reproducibility of the work that we publish. This form provides structure for consistency and transparency in reporting. For further information on Nature Portfolio policies, see our Editorial Policies and the Editorial Policy Checklist.

Statistics

For all statistical analyses, confirm that the following items are present in the figure legend, table legend, main text, or Methods section.

n/a	Confirmed
☐	☒ The exact sample size (*n*) for each experimental group/condition, given as a discrete number and unit of measurement
☐	☒ A statement on whether measurements were taken from distinct samples or whether the same sample was measured repeatedly
☐	☒ The statistical test(s) used AND whether they are one- or two-sided *Only common tests should be described solely by name; describe more complex techniques in the Methods section.*
☒	☐ A description of all covariates tested
☐	☒ A description of any assumptions or corrections, such as tests of normality and adjustment for multiple comparisons
☐	☒ A full description of the statistical parameters including central tendency (e.g. means) or other basic estimates (e.g. regression coefficient) AND variation (e.g. standard deviation) or associated estimates of uncertainty (e.g. confidence intervals)
☐	☒ For null hypothesis testing, the test statistic (e.g. *F*, *t*, *r*) with confidence intervals, effect sizes, degrees of freedom and *P* value noted *Give P values as exact values whenever suitable.*
☒	☐ For Bayesian analysis, information on the choice of priors and Markov chain Monte Carlo settings
☒	☐ For hierarchical and complex designs, identification of the appropriate level for tests and full reporting of outcomes
☒	☐ Estimates of effect sizes (e.g. Cohen's *d*, Pearson's *r*), indicating how they were calculated

Our web collection on statistics for biologists contains articles on many of the points above.

Software and code

Policy information about availability of computer code

Data collection	PROSize 3.0 (Agilent Technologies), Tecan Safire 2 Microplate Reader, SpectraMax 190 Microplate Reader, S6 FluoroSpot Analyzer (CTL, Shaker Heights OH), Symphony A3 Lite (BD), CTL ImmunoSpot®, IVIS Spectrum imaging system (Caliper Life Sciences), Victor3 1420 Multilabel Plate Counter (Perkin Elmer), Q-Exactive Orbitrap MS coupled to a Thermo Vanquish LC, G8 PET/CT scanner (PerkinElmer), LSR II flow cytometer (BD Biosciences), NxT Attune flow cytometer (ThermoFisher Scientific), Aurora (Cytek), FLEXMAP 3D (Luminex), LSM 710 (Zeiss), X-Light V3 Spinning Disk (CrestOptics).
Data analysis	FlowJo v10, ImmunoSpot®, Living IMAGE Software (Caliper), Imalytics software (version 3.1.1.6, Gemse-IT GmbH), SpectroFlow v2.2 (Cytek), Luminex® xPONENT® 4.2, Bio-Plex Manager™ Software 6.1, GraphPad Prism® v10.0.0, Microsoft® Excel® for Microsoft 365 MSO (Version 2411 Build 16.0.18227.20082, ImageJ2 (Fiji) version 1.54p open source software (BIOP JaCOP plugin).

For manuscripts utilizing custom algorithms or software that are central to the research but not yet described in published literature, software must be made available to editors and reviewers. We strongly encourage code deposition in a community repository (e.g. GitHub). See the Nature Portfolio guidelines for submitting code & software for further information.

Data

Policy information about availability of data

All manuscripts must include a data availability statement. This statement should provide the following information, where applicable:

- Accession codes, unique identifiers, or web links for publicly available datasets
- A description of any restrictions on data availability
- For clinical datasets or third party data, please ensure that the statement adheres to our policy

The primary datasets, along with detailed results of all statistical analyses, are provided in the Source Data files.

Research involving human participants, their data, or biological material

Policy information about studies with human participants or human data. See also policy information about sex, gender (identity/presentation), and sexual orientation and race, ethnicity and racism.

Reporting on sex and gender	Primary human monocytes were obtained from anonymous healthy apheresis donors at the University of Pennsylvania Human Immunology Core. HIC RRID: SCR_022380
Reporting on race, ethnicity, or other socially relevant groupings	Primary human monocytes were obtained from anonymous healthy apheresis donors at the University of Pennsylvania Human Immunology Core. HIC RRID: SCR_022380
Population characteristics	Primary human monocytes were obtained from anonymous healthy apheresis donors at the University of Pennsylvania Human Immunology Core. HIC RRID: SCR_022380
Recruitment	Primary human monocytes were obtained from anonymous healthy apheresis donors at the University of Pennsylvania Human Immunology Core. HIC RRID: SCR_022380
Ethics oversight	All primary human monocytes were covered through approval by the University of Pennsylvania Institutional Review Board (IRB). All de-identified donors signed approved consent forms.

Note that full information on the approval of the study protocol must also be provided in the manuscript.

Field-specific reporting

Please select the one below that is the best fit for your research. If you are not sure, read the appropriate sections before making your selection.

☒ Life sciences ☐ Behavioural & social sciences ☐ Ecological, evolutionary & environmental sciences

For a reference copy of the document with all sections, see nature.com/documents/nr-reporting-summary-flat.pdf

Life sciences study design

All studies must disclose on these points even when the disclosure is negative.

Sample size	No statistical methods were used to calculate the sample size. Sample size was determined based on previous experience: Alameh MG et al. Immunity. doi: 10.1016/j.immuni.2021.11.001.
Data exclusions	Figure 2. In the LNP W group, one animal displayed an extremely low event count, and that particular animal was excluded from the LLPC analysis. Figure 3. In cases of misinjection of CD8+ and Thy1.1+ T cells data were excluded.
Replication	In this study, 4 to 9 biological replicates were used for statistical comparisons in in vivo experiments. Neutralization assays and ELISA were performed in duplicate, and all replicates produced consistent results. For in vitro experiments, a minimum of three technical replicates were included. For both in vivo and in vitro studies, all attempts at replication were successful.
Randomization	For all experiments, mice were allocated randomly to the control and experiment groups. For ELISA, all samples were randomized to ensure that no two samples from the same group were placed on the same microtiter plate.
Blinding	Investigators were blinded to sample groups during data collection by labeling samples with generic numbers, ensuring that group identities remained unknown.

Reporting for specific materials, systems and methods

We require information from authors about some types of materials, experimental systems and methods used in many studies. Here, indicate whether each material, system or method listed is relevant to your study. If you are not sure if a list item applies to your research, read the appropriate section before selecting a response.

Materials & experimental systems

n/a	Involved in the study
☐	☒ Antibodies
☐	☒ Eukaryotic cell lines
☒	☐ Palaeontology and archaeology
☐	☒ Animals and other organisms
☒	☐ Clinical data
☒	☐ Dual use research of concern
☒	☐ Plants

Methods

n/a	Involved in the study
☒	☐ ChIP-seq
☐	☒ Flow cytometry
☒	☐ MRI-based neuroimaging

Antibodies

Antibodies used

RBD specific IgG Endpoint ELISA, IgG subtypes and IgA: HRP-conjugated anti-mouse IgG (Polyclonal, Jackson Immunoresearch #115-035-003), HRP-conjugated anti-mouse IgG1(polyclonal, abcam, AB 98693), HRP-conjugated anti-mouse IgG2a (polyclonal, abcam, AB98698), HRP-conjugated anti-mouse IgG2b (polyclonal, abcam, AB98703), HRP-conjugated anti-mouse IgA (polyclonal, abcam, AB97235).

HA specific IgG Quantitative ELISA: anti-HA (Clone #2F1A7, SinoBiological #11684-MM03), HRP-conjugated anti-mouse secondary antibody (Polyclonal, Jackson Immunoresearch, #115-036-071)

FRNT pseudovirus assay: mouse anti-VSV Indiana G (clone 1E9F9, Absolute Antibody, Ab01402-2.0)

Flow cytometry analysis of MBCs/LLPCs in mouse splenocytes and bone marrow: anti-B220 (APC, clone RA3-6B2, Tonbo, 20-0452), anti-CD138 (BB700, clone 281-2, BD Biosciences, 742124), anti-CD38 (AF700, clone 90, Invitrogen, 56-0381-82), anti-IgD (APC-Cy7, clone 11-26C.2A, Biolegend, 405716), anti-CD19 (BV785, clone 6D5, Biolegend, 115543), anti-GL7 (AF488, clone GL7, Biolegend, 144608), anti-CD4 (PE-Cy7, clone GK1.5, Biolegend, 100422), anti-CD8a (PE-Cy7, clone 53-6.7, Biolegend, 100722), anti-Ter-119 (PE-Cy7, clone TER119, Biolegend, 116222), anti-F4/80 (PE-Cy7, clone BM8, Biolegend, 123114).

ELISPOT Assay: anti-IgG1 (biotin, polyclonal, Southern Biotech, 1070-08), anti IgG2a (biotin, polyclonal, Southern Biotech, 1080-08), anti-IgG2b (biotin, polyclonal, Southern Biotech, 1090-08)

Spike Specific CD4+ and CD8+ T cell studies: Anti-Mouse CD16/CD32 (Fc Block) (BD Biosciences, clone 2.4G2, 553142), Live/dead fixable aqua (Life Technologies, L34957), anti-CD4 (PerCP/Cy5.5, clone GK1.5, BioLegend, 100434), anti-CD8 (Pacific Blue, clone 53-6.7, BioLegend, 100725), anti-CD3 (APC-Cy7, clone 145-2C11, BD Biosciences, 561042), anti-TNF-α (PE-Cy7, clone MP6-XT22, BD Biosciences, 557644), and anti-IFN-γ (AF700, clone XMG1.2, BD Biosciences, 557998)

Gp100-specific CD8+ T cell studies: Anti-CD3 (PerCP/Cyanine5.5, clone 17A2, Biolegend, #100218), anti-CD3 (APC, clone 145-2C11, Biolegend, #100312), anti-CD8 (PE/Cyanine7, clone 53-6.7, Biolegend, #100722), anti-CD90.1 (Thy1.1) (FITC, clone OX-7, Biolegend, #202504), anti-KLRG1 (PE, clone 2F1/KLRG1, Biolegend, #138408), anti-CD127 (IL-7Rα) (APC/Cyanine7, clone A7R34, Biolegend, #135040), anti-CD27 (APC, clone LG.3A10, Biolegend, #124212), anti-IFN-γ (PE, clone XMG1.2, Biolegend, #505808), anti-IFN-γ (Brilliant Violet 421, clone XMG1.2, Biolegend, #505830), anti-TNF-α (Brilliant Violet 711, clone MP6-XT22, Biolegend, #506349). Infiltration and vivo cellular uptake by DCs, monocytes and macrophages in the dLNs (Sup Fig 13-14): Anti I-A/I-E (BUV805, clone M5/114.15.2, BD, 748844), anti-CD11b (BV421, clone M1/70, Biolegend, 101236), anti-TCRb (BV510, clone H57-597, Biolegend, 109234), anti-CD317 (BV605, clone 927, Biolegend, 127025), anti-Ly6G (BV650, clone 1A8, Biolegend, 127641), anti-CD103 (BV785, clone 2E7, Biolegend, 121439), anti-Ly6C (PerCP-Cy5.5, clone HK1.4, Invitrogen, 45-5932-82), anti-CD19 (PE-Cy5, clone 6D5, Biolegend, 115510), anti-CD11c (PE-Cy-7, clone N418, Biolegend, 117318), anti-CD170 (APC, clone S17007L, Biolegend, 155508), anti-CD326 (AF700, G8.8, Biolegend, 118240), Live/dead (eFluor 780, eBioScience, 115-095-020).

Innate immune cell infiltration to muscle injection site: Anti-CD11c (BV421, clone N418, Biolegend, 117330), anti-CD45 (BV605, clone 30-F11, Biolegend, 103139), anti-I-A/I-E (BV650, clone M5/114.15.2, BD Biosciences, 563415), anti-CD24 (BV711, clone M1/69, BD Biosciences, 563405), anti-CD11b (APC-Cy7, clone M1/70, BD Biosciences, 557657), anti-Ly6-G (AF700, clone 1A8, BD Biosciences, 561236), anti-CD64 (PE-CF594, clone X54-5/7.1, Biolegend, 139320), anti-F4/80 (PE, clone BM8, Biolegend, 123109), anti- CD16/CD32 (Fc block) (BD Biosciences, clone 2.4G2, 553142).

Endosomal escape study: anti-EEA1 (polyclonal, ThermoFisher, cat# PA1063A), anti-LAMP1 (polyclonal, ThermoFisher, cat# PA1654A), Rabbit IgG Isotype Control (Polyclonal, ThermoFisher, cat# 31235), F(ab')2-Goat anti-Rabbit IgG (H+L) (Alexa Fluor 488, ThermoFisher, cat# A11070).

Validation

All antibodies used in this study are commercially available, and all have been validated by the manufacturers and used by other publications. All antibodies used for flow cytometry were quality control tested by immunofluorescent staining with flow cytometric analysis.

Primary antibody validation:
HRP-conjugated anti-mouse IgG (Polyclonal, Jackson Immunoresearch #115-035-003). Validation statements for the species on the manufacturer's website: "Based on immunoelectrophoresis and/or ELISA, the antibody reacts with whole molecule mouse IgG. It also reacts with the light chains of other mouse immunoglobulins. No antibody was detected against non-immunoglobulin serum proteins. The antibody may cross-react with immunoglobulins from other species." Reference: Wei SC et al. 2021, Front Immunol. doi: 10.3389/fimmu.2021.771011.

HRP-conjugated anti-mouse IgG1(polyclonal, abcam, AB 98693). Validation statements for the species on the manufacturer's

website: "By immunoelectrophoresis and ELISA this antibody reacts specifically with mouse IgG1. Cross reactivity with immunoglobulins is less than 2%. No antibody was detected against non-immunoglobulin serum proteins. Less than 1% cross reactivity to human and rat IgG1 was detected. This antibody may cross react with IgG1 from other species." Reference: Han X et al. 2023, Nat Nanotechnol. doi: 10.1038/s41565-023-01404-4.

HRP-conjugated anti-mouse IgG2a (polyclonal, abcam, AB98698). Validation statements for the species on the manufacturer's website: "By immunoelectrophoresis and ELISA this antibody reacts specifically with mouse IgG2a. Cross reactivity with immunoglobulins is less than 2%. No antibody was detected against non-immunoglobulin serum proteins. Less than 1% cross reactivity to human and rat IgG2a was detected. This antibody may cross react with IgG2a from other species." Reference: Nardo D et al. 2022, Biomater Sci. doi: 10.1039/d2bm01289h.

HRP-conjugated anti-mouse IgG2b (polyclonal, abcam, AB98703). Validation statements for the species on the manufacturer's website: "Target species, Mouse. Suitable for ICC, IHC-P, ELISA, WB. Ideal for western blot. Preadsorbed to minimise non-specific binding and high background staining." Reference: Nardo D et al. 2022, Biomater Sci. doi: 10.1039/d2bm01289h.

HRP-conjugated anti-mouse IgA (polyclonal, abcam, AB97235). Validation statements for the species on the manufacturer's website: By immunoelectrophoresis and ELISA this antibody reacts specifically with Mouse IgA. Cross reactivity with other immunoglobulins and light chains is less than 0.1%. Cross reactivity to mouse IgM, IgG1, IgG2a, IgG2b, IgG2c, IgG3 and IgE is undetectable. Some hybridoma clones may express aberrant immunoglobulin-related peptides that are improperly recognized by this antibody." Reference: Muranishi K et al. 2023, Vaccines, doi: 10.3390/vaccines12010005.

anti-HA (Clone #2F1A7, SinoBiological #11684-MM03). Validation statements for the species on the manufacturer's website: "Specificity, H1N1 (A/Puerto Rico/8/1934) H, has cross-reactivity in ELISA with H1N1 (A/Puerto Rico/8/1934) HA Protein (Cat# 11684-V08H)" Reference: Yu L et al. 2024. Virol Sin. doi: 10.1016/j.virs.2024.01.003.

anti-VSV Indiana G (clone 1E9F9, Absolute Antibody, Ab01402-2.0). Validation statements for the species on the manufacturer's website: "Specificity: VSV-Ind glycoprotein (G) protein" Reference: Tam AB et al. 2018, Dev Cell. doi: 10.1016/j.devcel.2018.04.023.

anti-IgG1 (biotin, polyclonal, Southern Biotech, 1070-08). Validation statements for the species on the manufacturer's website: "Specificity Reacts with the heavy chain of mouse IgG1" Reference: Koutsonanos DG et al. 2025, Vaccine. doi: 10.1016/j.vaccine.2015.01.086.

anti-IgG2a (biotin, polyclonal, Southern Biotech, 1080-08). Validation statements for the species on the manufacturer's website: "Specificity: Reacts with the heavy chain of mouse IgG2a" Reference: Teichmann LL et al. 2013, Immunity. doi: 10.1016/j.immuni.2012.11.017.

anti-IgG2b (biotin, polyclonal, Southern Biotech, 1090-08). Validation statements for the species on the manufacturer's website: "Specificity: Reacts with the heavy chain of mouse IgG2b" Reference: Hsu HC et al. 2007, J Immunol. doi: 10.4049/jimmunol.178.8.5357.

anti-EEA1 (polyclonal, ThermoFisher, cat# PA1063A). Validation statements for the species on the manufacturer's website: "Species Reactivity Human, Mouse " Reference: Aung KT et al. 2019, J Physiol Sci. doi: 10.1007/s12576-018-0644-2.

anti-LAMP1 (polyclonal, ThermoFisher, cat# PA1654A). Validation statements for the species on the manufacturer's website: Species Reactivity Human. Reference: (mouse and human) Donde A et al. 2019 doi: 10.1080/15548627.2019.1635379.

Eukaryotic cell lines

Policy information about cell lines and Sex and Gender in Research

Cell line source(s)	Murine DC2.4 cell line was obtained from Millipore Sigma (#SCC142M) the American Type Culture Collection and maintained in Dulbecco's modified Eagle's medium (DMEM, Corning, #10-013-CV) supplemented with 10% fetal bovine serum (Cytivia Hyclone, #SH30071.03), 100 U ml−1 Penicillin/Streptomycin (Gibco. #15140-122).RPMI complete media [RPMI 1640 (Gibco) supplemented with 10% Fetal Bovine Serum (Cytivia Hyclone), and 1% Penicillin/Streptomycin (Gibco)]. Human monocyte-derived dendritic cells were generated from a healthy donor apheresis product, provided by the University of Pennsylvania Human Immunology Core (SCR_022380). Dendritic cells were derived from monocytes using complete RPMI complete media (Gibco, #22400-089) supplemented with human granulocyte colony stimulating factor (R&D Ssystems, #215GM010CF) and human IL-4 (R&D Ssystems, #204IL010CF). Expi293F cells were obtained from Thermo Fisher Scientific (#A14527) and maintained in Expi293™ Expression Medium (Thermo Fisher Scientific, #A1435101). Sf9 cells were obtained from Thermo Fisher Scientific (#12659017) and maintained in Sf-900™ III SFM, a serum-free medium (Thermo Fisher Scientific, #12658019), supplemented with 1× Penicillin-Streptomycin (Capricorn, 100× stock solution). High Five cells were obtained from Thermo Fisher Scientific (#B85502) and maintained in HyClone™ SFX-Insect liquid medium (Cytiva, #SH30278.LS). 293T cells were obtained from the American Type Culture Collection (ATCC, #CRL-3216) and maintained in DMEM (Life Technologies, #11995065) supplemented with 10% fetal bovine serum (Hyclone, #SH30071.03). VeroE6-TMPRSS2 cells were generated in-house, selected once with blasticidin (#R21001), and maintained in DMEM (Life Technologies, #11995065).
Authentication	Human monocyte-derived dendritic cells were generated from a healthy donor apheresis product provided by the University of Pennsylvania Human Immunology Core (SCR_022380). Monocytes were differentiated into dendritic cells using RPMI complete medium supplemented with human granulocyte-macrophage colony-stimulating factor (GM-CSF; R&D Systems, 215-GM-010CF) and human interleukin-4 (IL-4; R&D Systems, 204-IL-010CF). Authentication was based on cellular morphology, characterized by large, irregularly shaped cells with long dendrite-like projections, a prominent indented nucleus, and clear cytoplasm. The authentication of DC2.4 cells was performed by the manufacturer based on characteristic features of dendritic cells

including cell morphology and the expression of dendritic cell-specific markers and the ability to phagocytose and present exogenous antigens on both MHC class I and class II molecules.

Expi293F cells (Cat# A14527, Thermo Fisher Scientific, Waltham, MA, USA):
The authentication of the Expi293F cell line was performed and documented by the manufacturer, based on morphology and growth characteristics consistent with human HEK293-derived suspension cell lines.

Sf9 cells (Cat# 12659017), Thermo Fisher Scientific, Waltham, MA, USA): The authentication of the Sf9 cell line was performed and documented by the manufacturer, based on morphology and growth characteristics consistent with Spodoptera frugiperda-derived PLB-Sf-21-AE insect cell lines.

High Five cells (Cat# B85502), Thermo Fisher Scientific, Waltham, MA, USA): The authentication of the High Five cell line was performed and documented by the manufacturer, based on morphology (large spherical cells with some granular appearance) and growth characteristics consistent with Trichoplusia ni-derived BTI-TN-5B1-4 insect cell lines.

293T cells (CRL-3216), ATCC: The authentication of 293 cells was performed by the manufacturer through Short Tandem Repeat (STR) profiling (D3S1358: 15,17; TH01: 7,9.3; D21S11: 28,30.2; D18S51: 17,18; Penta_E: 7,15; D5S818: 8,9; D13S317: 12,14; D7S820: 11; D16S539: 9,13; CSF1PO: 11,12; Penta_D: 9,10; Amelogenin: X; vWA: 16,19; D8S1179: 12,14; TPOX: 11; FGA: 23; D19S433: 18.; D2S1338: 19.

VeroE6-TMPRSS2 cells were generated in-house, authenticated based on characteristic epithelial morphology and expected growth behavior, including adherent, cobblestone-like appearance and consistent proliferation rate, selected once with blasticidin (Invitrogen).

Mycoplasma contamination: All cell lines were routinely tested and confirmed to be negative for mycoplasma contamination.

Commonly misidentified lines (See ICLAC register): No commonly misidentified cell lines were used in the study.

Animals and other research organisms

Policy information about studies involving animals; ARRIVE guidelines recommended for reporting animal research, and Sex and Gender in Research

Laboratory animals	BALB/c mice aged 8 weeks were purchased from Charles River Laboratories. C57BL/6J (Jackson Laboratory strain #000664) and Pmel-1 TCR/Thy1.1 transgenic mice Jackson Laboratory strain #005023) on a C57BL/6 background (aged 6–8 weeks) were purchased from the Jackson Laboratory. Pmel-1 mice were bred and maintained at the University of California, Los Angeles (UCLA). Breeding vivarium and utilized for experiments when reaching 8 to 12 weeks of age.
Wild animals	No wild animals were used in this study.
Reporting on sex	Female mice were used in this study.
Field-collected samples	No filed-collected samples were used in this study.
Ethics oversight	The investigators faithfully adhered to the "Guide for the Care and Use of Laboratory Animals" by the Committee on Care of Laboratory Animal Resources Commission on Life Sciences, National Research Council. Mouse studies were conducted under protocols approved by the Institutional Animal Care and Use Committees (IACUC) of the University of Pennsylvania, the University of California, Los Angeles, and Genevant. All animals were housed and cared for according to local, state, and federal policies in an Association for Assessment and Accreditation of Laboratory Animal Care International (AAALAC)-accredited facility.

Note that full information on the approval of the study protocol must also be provided in the manuscript.

Plants

Seed stocks	*Report on the source of all seed stocks or other plant material used. If applicable, state the seed stock centre and catalogue number. If plant specimens were collected from the field, describe the collection location, date and sampling procedures.*
Novel plant genotypes	*Describe the methods by which all novel plant genotypes were produced. This includes those generated by transgenic approaches, gene editing, chemical/radiation-based mutagenesis and hybridization. For transgenic lines, describe the transformation method, the number of independent lines analyzed and the generation upon which experiments were performed. For gene-edited lines, describe the editor used, the endogenous sequence targeted for editing, the targeting guide RNA sequence (if applicable) and how the editor was applied.*
Authentication	*Describe any authentication procedures for each seed stock used or novel genotype generated. Describe any experiments used to assess the effect of a mutation and, where applicable, how potential secondary effects (e.g. second site T-DNA insertions, mosiacism, off-target gene editing) were examined.*

Flow Cytometry

Plots

Confirm that:

☒ The axis labels state the marker and fluorochrome used (e.g. CD4-FITC).

☒ The axis scales are clearly visible. Include numbers along axes only for bottom left plot of group (a 'group' is an analysis of identical markers).

☒ All plots are contour plots with outliers or pseudocolor plots.

☒ A numerical value for number of cells or percentage (with statistics) is provided.

Methodology

Sample preparation	Flow cytometry analysis of MBCs/LLPCs in mouse splenocytes and bone marrow: Splenocytes were harvested from spleens by mechanical disruption between frosted slides and filtered through 63-micron Nitex mesh. Bone marrow was flushed from femurs and tibia from each mouse using a 23g X ¾" needle and syringe into FACS buffer (PBS + 2% fetal bovine serum) and filtered through 63-micron Nitex mesh. Red blood cells were lysed with ACK Lysing buffer (Lonza #10-548E) for 5 minutes on ice and the reaction was stopped with ten times the volume of PBS. Five million cells were then stained with fixable live dead aqua (Biolegend Zombie Aqua, 423101 – 1:500 in PBS) for 15 min at RT. Cells were then washed with FACS buffer and stained with the respective dilutions of antibodies in BD Brilliant Staining Buffer (BD Biosciences, 563794) for 15 min at 4 °C. To create fluorescently labeled RBD tetramers, recombinant RBD was biotinylated using the EZ-Link Micro Sulfo-NHS-Biotinylation Kit (ThermoFisher). Streptavidin-conjugated Alexa PE and Alexa Flour 647 (all from Biolegend) were then added at a 6:1 molar ratio (biotinylated-protein to streptavidin-conjugate). Specifically, after the volume of fluorochrome needed to achieve a 6:1 molar ratio was determined, the total volume of fluorochrome was split into 10 subaliquots. These subaliquots were then added, on ice, to the biotinylated protein and mixed by pipetting every 10 minutes (for a total of 10 additions). Gp100-specific CD8+ T cell studies: Peripheral blood was obtained from mice through retro-orbital eye bleeds under anesthesia and collected into 1.5 ml Eppendorf tubes containing 2 µl of 0.5 M EDTA to inhibit coagulation. Blood samples were subjected to three cycles of red blood cell lysis using 500 µL of ACK lysis buffer each cycle. Samples were resuspended in FACS buffer (1 x PBS containing 5% FBS and 2 mM EDTA), passed through a 70 µm filter to remove debris, counted, and finally allocated for downstream flow cytometric analyses or functional assays. For Intracellular Cytokine Staining (ICS) and Flow Cytometry analyses, PBMCs were plated at 1 × 105 cells per well in a 96-well round bottom plate and re-stimulated for 5 hours with the murine gp10025-33 epitope (EGSRNQDWL) peptide at 1 µg/ml in complete RPMI 1640 medium (supplemented with 10% FBS, 1% penicillin/streptomycin and 55 µM β-mercaptoethanol) at 37 °C in the presence of brefeldin-A (15 µg/ml). After 5 hours, cells were collected and stained Infiltration and vivo cellular uptake by DCs, monocytes and macrophages in the dLNs: For DC analysis, draining LNs were harvested, disrupted with scissors, and then digested in RPMI + 2% FBS + 20mM HEPES + 400U/mL type-IV collagenase for 30 minutes at 37 °C. LNs were then passed through a 21G x 1 syringe (BD 309624) 5 times before being filtered through a 40uM mesh filter. Staining steps were all performed at 4°C in FACS Buffer (PBS + 2% FBS + 5mM EDTA). Prior to staining, single-cell suspensions were Fc blocked with anti-mouse CD16/CD32 blocking antibody at 1:1000 (~7.6 µg /mL). Cells were washed and then incubated for 30 minutes with a cocktail of viability dye and fluorescently labeled antibodies. Innate immune cell infiltration to muscle injection site: Tissue was minced and subsequently digested using of 10 ml XMedia [Ham's F12 Nutruent Mix (Gibco), 10% FBS (Cytivia Hyclone), and 100 units/ml penicillin and 100 mg/ml streptomycin (Gibco)] containing 100 units/ml collagenase, type IV (Gibco) and 1.1 units/ml dispase II (Roche) for 30 minutes at 37 °C while shaking. Supernatant from enzymatic digestion was filtered through a 70 µm cell strainer and washed with PBS. Filtering and PBS wash was repeated, and samples resuspended in 1 ml of XMedia. 3 million cells per sample were used for flow cytometry staining. Samples were washed with PBS and stained with a LIVE/DEAD Fixable Aqua Dead Cell Stain Kit (Life Technologies) for 10 minutes in the dark at room temperature. Cells were subsequently incubated for 30 minutes at 4 °C with a master mix of fluorescently labeled anti-mouse monoclonal antibodies.
Instrument	Symphony A3 Lite (BD), LSR II flow cytometer (BD Biosciences), NxT Attune flow cytometer (ThermoFisher Scientific), Aurora (Cytek)
Software	FlowJo analysis software v10
Cell population abundance	The average MBC abundance ranges between 21.4% and 41.1% of splenocytes. The average LLPC abundance ranges from 7.4% to 22.2% of bone marrow cells. The average abundance of Spike-specific CD8+ IFN-γ+ cells ranges from 1.5% to 3.3%, Spike-specific CD8+ TNF-α+ cells range from 0.3% to 1.2%, and Spike-specific CD8+ TNF-α+ IFN-γ+ cells range from 0.2% to 0.8% within the CD3+CD8+ population. Within the CD3+CD4+ population, the average abundance of Spike-specific CD4+ IFN-γ+ cells ranges from 0.16% to 0.17%, CD4+ TNF-α+ cells from 0.26% to 0.3%, and CD4+ TNF-α+ IFN-γ+ cells from 0.10% to 0.12%. The average abundance of Gp100-specific CD8+ Thy1.1+ IFN-γ+ cells ranges from 73% to 76%, Gp100-specific CD8+ Thy1.1+ TNF-α+ cells range from 22% to 29%, and Gp100-specific CD8+ Thy1.1+ IFN-γ+ TNF-α+ cells range from 21% to 28% within the CD8+ Thy1.1+ T cell population following a prime and bolus immunization regimen.

The average abundance of Gp100-specific CD8+ Thy1.1+ IFN-γ+ cells ranges from 86% to 87%, Gp100-specific CD8+ Thy1.1+ TNF-α+ cells range from 43% to 48%, and Gp100-specific CD8+ Thy1.1+ IFN-γ+ TNF-α+ cells range from 27% to 34% within the CD8+ Thy1.1+ T cell population. Gp100-specific CD8+ Thy1.1+ KLRG1+ CD127- cells range from 7.4% to 10% within the CD3+CD8+ Thy1.1+ population following extended prime immunization regimen.

The average absolute number ($\times 10^4$) in the LN of total DCs ranges from 2.6 to 5.0, dermal DCs range from 0.4 to 1.17, cDC1 cells range from 0.1 to 0.5, cDC2 cells range from 0.5 to 1.7, pDCs range from 0.8 to 2.6, inflammatory monocytes range from 0.3 to 3.2, and macrophages range from 1.6 to 3.2.

The average abundance of EGFP+ DiI+ dermal DCs ranges from 2.5% to 5.4%, EGFP+ DiI+ cDC1s from 5.9% to 13.6%, EGFP+ DiI+ cDC2s from 8.5% to 16.1%, EGFP+ DiI+ pDCs from 0.3% to 1.3%, EGFP+ DiI+ inflammatory monocytes from 0.1% to 0.3%, and EGFP+ DiI+ macrophages from 0.2% to 0.6%.

The average abundance in the injection site muscle of neutrophils ranges from 1.9% to 19.4%, DCs from 0.8% to 6.5%, macrophages from 0.1% to 2.8%, and monocytes from 0.4% to 5.6% within the CD45+ cell population.

Gating strategy

Flow Cytometric Gating Strategy for the Investigation of MBC: (IgD−Dump[CD4,CD8a,Ter-119, F4/80]−CD19+B220+CD38+GL7−RBD-AF647+/RBD-PE+), Antigen-specific LLPCs (IgD−Dump[CD4, CD8a, Ter-119, F4/80]-B220−CD138+RBD-AF647+/RBD-PE+)

Flow Cytometric Gating Strategy for the Investigation of spike-specific CD4+ and CD8+ T cell responses: Singlets cells were first selected (FSC-H x FSC-A), then live cells (LD-), lymphocytes were selected based on size and granularity (FSC x SSC), and the cytokine production was evaluated inside the CD3+CD4+ and CD3+CD8+ populations.

Flow cytometric gating strategy for the investigation of gp100-specific CD8+ T cell responses: Singlets cells were first selected (FSC-H x FSC-A), then live cells (LD-), and the cytokine production (TNFa+ and/or IFNg+) was evaluated in the T cells CD8+ Thy1.1+. Singlets cells were first selected (FSC-H x FSC-A/ SSC-H x SSC-A), then live cells (LD-), and cytotoxic profile was evaluated in CD3+CD8+ Thy1.1+ cells based on KLRG1 and CD127 markers expression.

Flow cytometric gating strategy for assessing the cellular populations and mRNA-LNP uptake in dLNs: Single cells were selected based on size and granularity (FSC x SSC), then live cells (LD-), and then DCs subsets were defined: cDC1s (CD11b +MHCII+EpCAM-CD103+), cDC2s (CD11b+MHCII+EpCAM-CD11b+) and pDCs (CD11b-PDCA1+). From CD11b+ cells, Monocytes subset (Ly-6G- SiglecF- Ly6C+) and Macrofages subset (Ly-6G- SiglecF- Ly6C-) were also defined.

Flow cytometric gating strategy for assessing innate cell populations in injection site muscle of immunized mice: Single cells were selected based on size and granularity (FSC x SSC), then live cells (LD-) and in Leykocytes (CD45+) subset, innate cells were defined as neutrophils (Ly6G+), Macrophages (Ly6G-CD11b+SSChiCD64+), Dendritics cells (Ly6G-CD11c+MHC+CD24+) and Monocytes (Ly6G-CD11b+MHC-F4/80+)

☒ Tick this box to confirm that a figure exemplifying the gating strategy is provided in the Supplementary Information.